Universität Potsdam

Institut für Physik und Astronomie

Professur für Statistische Physik und Chaostheorie

Diplomarbeit

Localization Properties of Nonlinear Disordered Lattices

von

Mario Mulansky

Aufgabenstellung und Betreuung:

Prof. Dr. Arkady Pikovsky

Gutachter:

Prof. Dr. Arkady Pikovsky
Dr. habil. Carsten Henkel

eingereicht im **März 2009**

Zusammenfassung

In dieser Arbeit wird das Verhalten nichtlinearer Ketten mit Zufallspotential untersucht. Teil I enthält eine Einführung in das Phänomen der Anderson Lokalisierung, die Diskrete Nichtlineare Schrödinger Gleichung und ihren Eigenschaften sowie die verwendete Verallgemeinerung des Modells durch Einführung eines Nichtlinearitäts-Indizes α.

In Teil II wird das Ausbreitungsverhalten von lokalisierten Zuständen in langen, ungeordneten Ketten durch die Nichtlinearität untersucht. Dazu werden zuerst verschiedene Lokalisierungsmaße besprochen und außerdem die strukturelle Entropie als Messgröße der Peakstruktur eingeführt. Im Anschluss wird der Ausbreitungskoeffizient für verschiedene Nichtlinearitäts-Indizes bestimmt und mit analytischen Abschätzungen verglichen.

Teil III behandelt schließlich die Thermalisierung in kurzen, ungeordneten Ketten. Dabei wird zuerst der Begriff Thermalisierung in dem verwendeten Zusammenhang erklärt. Danach erfolgt eine numerische Analyse von Thermalisierungseigenschaften lokalisierter Anfangszustände, wobei die Energieabhängigkeit besondere Beachtung genießt. Eine Verbindung mit sogenannten Breathers wird dargelegt.

Abstract

In this thesis, the properties of nonlinear disordered one dimensional lattices is investigated. Part I gives an introduction to the phenomenon of Anderson Localization, the Discrete Nonlinear Schrödinger Equation and its properties as well as the generalization of this model by introducing the nonlinear index α.

In Part II, the spreading behavior of initially localized states in large, disordered chains due to nonlinearity is studied. Therefore, different methods to measure localization are discussed and the structural entropy as a measure for the peak structure of probability distributions is introduced. Finally, the spreading exponent for several nonlinear indices is determined numerically and compared with analytical approximations.

Part III deals with the thermalization in short disordered chains. First, the term thermalization and its application to the system in use is explained. Then, results of numerical simulations on this topic are presented where the focus lies especially on the energy dependence of the thermalization properties. A connection with so-called breathers is drawn.

Contents

List of Figures

1 Introduction

1.1 Motivation

Since the fundamental work of P. W. Anderson in 1958 [And58], in which he proved the *absence of diffusion* in random lattices, a lot of research has been addressed to this phenomenon, which was later called *Anderson localization*. The mechanisms behind this type of localization are well understood nowadays and in chapter 2 we try to give an overview of the known results. A more sophisticated and detailed recap can be found in [LR85], for example. Later on, a new mechanism was added to systems that exhibit Anderson localization: *Nonlinearity*. In the presence of nonlinearity, the natural question appears, whether the Anderson localization gets destroyed or not. Nonlinear systems also give rise to new phenomena, one of which are breathers – localized excitations that can also be found in discrete lattices. Thus, from this point of view, one could also ask if the nonlinear breathers are destroyed by the disorder, which is partly dealt with in part III.

The question of destruction of Anderson localization is exactly what will be investigated in this work. More precisely, we consider two different, nevertheless related, problems: In part II, we tried to find out whether an initially localized probability distribution will spread in a random lattice when nonlinearity is present. This setup was already addressed, for example, by Pikovsky and Shepelyansky in [PS08], where subdiffusive spreading was found. On the other hand, there are also results by Flach and Aubry [KKFA08] that claim the complete absence of diffusion in such systems. Thus, we try to clarify this issue by searching for conditions under which spreading might, or might not, be observed.

While in the first setup the lattice is considered to be infinitely large, in part III a different system is of interest. It will be investigated, whether the nonlinearity leads to a thermalization[1] of initially localized states. Special interest lies on the dependence of thermalization on the energy and shape of the initial state. We hope that the results for these short chains can help to understand the interplay between localization and nonlinearity.

[1] See chapter 8 for our understanding of "thermalization" and the relation of initially localized states in short random lattices.

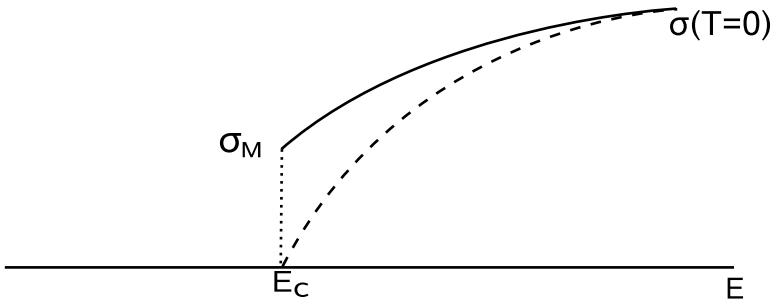

Figure 1.1: Schematic picture of the behavior of the zero temperature conductivity σ at the mobility edge E_c. Both possibilities for the Anderson transition, continuous and discontinuous with a jump of the conductivity at the mobility edge σ_M, are shown.

1.2 Experimental Observations

There are several experimental setups, partly of very different nature, where Anderson localization can be observed. In the following, a very brief overview of some experimental results on the most important systems is provided. For more details and results see, for example, the excellent review by Kramer and MacKinnon [KM93].

1.2.1 Anderson Transition

Historically, solid state systems were investigated first, as the conductivity can be related to the localization properties of the electrons in such setups. It was Mott who stated in 1967 the existence of a so called mobility edge E_c in two and three dimensional, moderately disordered electronic systems [Mot67]. This mobility edge separates localized from non-localized states by their energy. Note that in one dimension, all eigenstates are localized even if the disorder is arbitrarily small. Later, it was found by scaling arguments that in 2D systems all states must be localized, too. Now if the Fermi energy of a system lies in the localized regime, that is $E_F < E_c$, one expects vanishing zero temperature conductance while for $E_F > E_c$ the zero temperature conductance should be positive. This marks an insulator-metal–transition that depends on the localization properties of the electrons in the disordered system.

A very precise measurement of this transition was done by Paalanen, Rosenbaum, Thomas and Bhatt in 1982 [PRTB82], where a continuous metal-insulator transition was found in contrast to Mott's prediction of a discontinuity with a jump σ_M. Fig. 1.1 shows a schematic sketch of the two possibilities: continuous and discontinuous transition.

In a very recent experiment, Chabé et al. observed an Anderson transition with atomic matter waves [CLG$^+$08], where they stressed the correspondence between the quantum kicked rotor and the 3D Anderson model [She93].

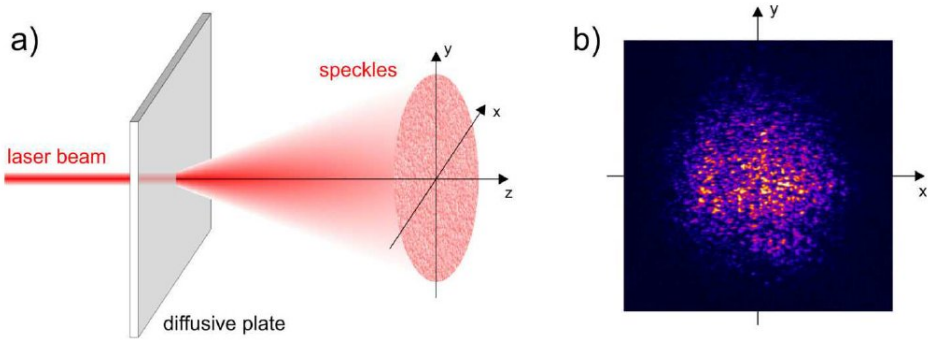

Figure 1.2: Production of speckle patterns. a) Laser beam shining through a diffusive plate creating a speckle pattern which can then be imaged onto a BEC. b) Typical intensity distribution of a speckle beam. Images taken from [FFI08].

Another notable result was obtained by von Molnar et al. [vMBFR83] in 1983. They investigated the metal–insulator transition for a magnetic semiconductor. The advantage of such a system is that it can be tuned continuously through the transition point via an external magnetic field. They also found the conductance being continuous at the transition point, which is, by the way, consistent with results from the scaling theory [LR85] developed later for the Anderson localization.

It should be mentioned here that the Anderson transition is a purely linear effect occurring in three dimensional systems of non–interacting electrons (or atoms). Therefore, the experiments mentioned above do not directly address the problems that are subject of this work.

1.2.2 Bose Einstein Condensates in Disordered Potentials

With the ability to create Bose Einstein Condensates (BECs), physicists nowadays have a powerful tool to investigate any type of quantum system [DGPS99]. One example are disordered systems with Anderson localization, which can be experimentally realized by ultracold atoms in an optical random potential. Hereby, the random potential is mostly created using speckle beams, firstly realized by Boiron et al. in 1999 [BMRF$^+$99]. Those speckles are produced by light being reflected by rough surfaces or transmitted through a diffusive medium as shown in Fig. 1.2. BECs and optical speckles have some outstanding features which make them very useful for investigating Anderson localization: Firstly, one has precise knowledge about the properties of the random potential, such as distribution width and spatial correlations. Secondly, the potential is static. And the last, most appealing, fact is that using BECs allows for a direct observation of localized states, whereas in other experiments only (macroscopic) consequences of Anderson localization are observed, e.g. conductivity. As a disadvantage, one should point out that these systems are usually two dimensional, but there exist methods to create one and three dimensional potentials as well. There are several experimental results showing Anderson localization of Bose Einstein Condensates in random potentials in both one and two dimensions [LFM$^+$05, CVH$^+$05, FFG$^+$05].

Furthermore, one gets naturally to the question of the influence of nonlinearity on Anderson localization by considering interacting BECs [SDK$^+$05]. Hence, those systems are particularly interesting as a direct application of the results of this work.

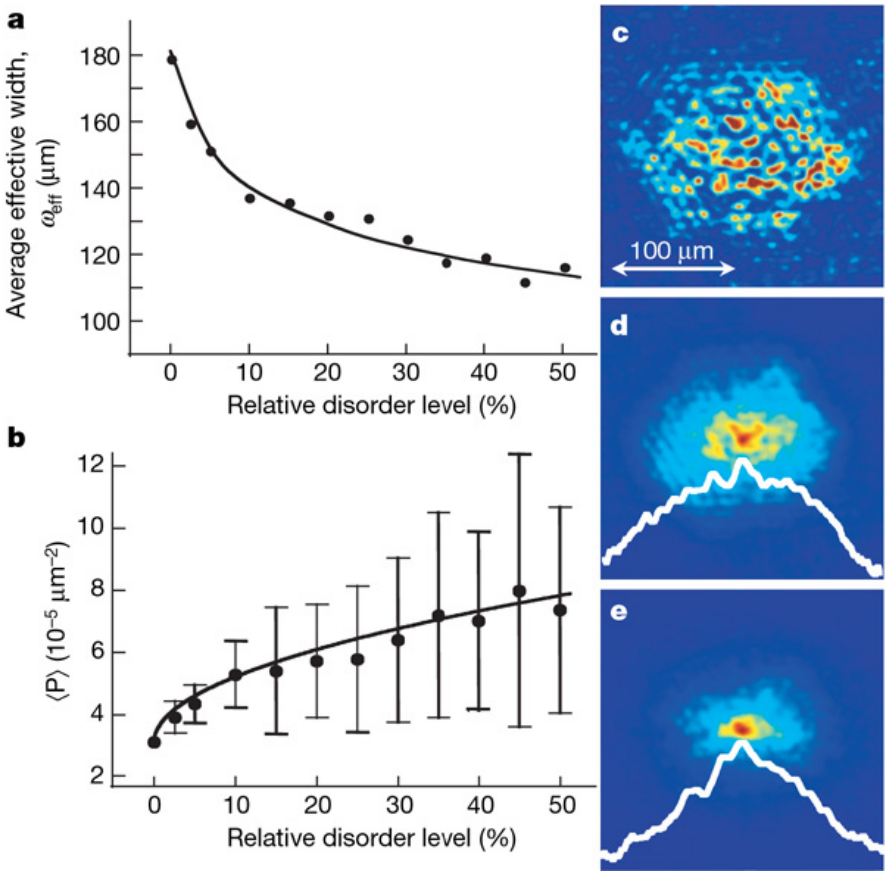

Figure 1.3: Experimental results for light in disordered photonic lattices obtained in [SBFS07]. The figure shows averaged effective width (a) and Participation Number (b) measured experimentally for different strengths of disorder. Averages were taken over 100 disorder realizations. Panels (c) - (e) show the intensity distributions for disorder levels of 0%, 15% and 45%, the white lines are averaged logarithmic intensities. The exponentially decaying intensity in panel (e) is interpreted as Anderson localization. (source: [SBFS07])

1.2.3 Light in Disordered Photonic Lattices

In 1984, John suggested the presence of localization of electromagnetic waves in strongly disordered media [Joh84]. Later, this was investigated in detail and Anderson localization was observed in an optical setup with strongly scattering semiconductor powders [WBLR97]. In a very recent experiment by Fishman et al. [SBFS07], the potential is created by a dielectric material that changes its refractive index when being exposed to an optical interference pattern. Thus, using a speckle beam as for BECs, the properties of the random potential can be controlled quite precisely. The results found in [SBFS07], which are shown in Fig. 1.3, support the existence of Anderson localization in those systems.

Furthermore, the effects of nonlinearity on Anderson localization can be studied using these kinds of systems. Some results on this can also be found in [SBFS07], indicating an increase of localization in the presence of self-focusing nonlinearity. However, when comparing these results with the conclusion drawn later in this text, one has to keep in mind that the experimental observations happened for completely different parameters and time-scales.

Part I

Nonlinear Disordered Lattices

2 Anderson Localization in Linear Systems

2.1 Understanding of Localization

First of all, the term *localization* needs to be clarified to ensure the reader's understanding of this work. The straightforward definition of localization is obtained by looking at the asymptotic behavior of a given wavefunction $\psi(\vec{r})$. We call ψ localized at $\vec{r}_0$ if its absolute square decreases exponentially at large distances from $\vec{r}_0$:

$$|\psi(\vec{r})|^2 = f(\vec{r}) \cdot \mathrm{e}^{-|\vec{r}-\vec{r}_0|/\xi}. \tag{2.1}$$

Here, f is some arbitrary subexponential[1] but positive function and ξ is called *localization length*.

Historically, first the diffusion or transport properties of a system were of interest rather than the asymptotic behavior of single wavefunctions. Thus in his pioneering article [And58] of 1958, P. W. Anderson did not use the term "localization", but rather proved the *Absence of Diffusion*. It seems very natural, and can be shown rigorously, that for a given (linear) system the transport properties at vanishing temperature depend on the character of the eigenstates around the Fermi energy E_F. If those states are extended, like for electrons in metals or free particles, one observes zero temperature transport through the system, hence diffusion. On the other hand, if the eigenstates of a system are known to be localized in the meaning of eq. (2.1), it can be shown that no diffusion is possible in the system. Thus, by knowing that the eigenstates around the Fermi energy are localized it can be concluded that there is no zero temperature diffusion. See section 2.3.3 for a more detailed analysis of this in 1D systems. Additionally, it is accepted that if absence of diffusion or vanishing conductance in a disordered system is experimentally observed, localization of the eigenstates can be concluded.

In the numerical simulations of part II of this work, the diffusion properties of a system are investigated by checking if an initially localized state remains localized over time in the presence of nonlinearity. To accomplish this, sophisticated techniques to measure the degree of localization are required, but a detailed discussion on this is delayed to chapter 5.

2.2 The Anderson Model

The Anderson model serves as the prototype of a system exhibiting localization due to disorder. In its original form, it can be written in terms of a Hamiltonian:

$$H = \sum_i E_i a_i^* a_i + \sum_{i \neq j} T_{ij} a_i^* a_j \tag{2.2}$$

[1] A subexponential function $f(x)$ is defined to increase slower than exponentially: $f(x)/\mathrm{e}^x \underset{x\to\infty}{\longrightarrow} 0$.

Where i, j refer to some kind of lattice indices and a_i is the complex valued excitation amplitude of an entity placed at the lattice site i, e.g. a spin. E_i is the energy of such a spin and a *random variable* distributed uniformly over an interval of width W. T_{ij} are the transfer (or hopping) matrix elements defining the interaction between spins at sites i and j. For such a system in a 3D lattice, Anderson proved the absence of diffusion under some restrictions on the interaction. His result goes as follows: If the interaction T_{ij} is sufficiently short ranged, that means decaying faster than $1/r^3$ for sites with distance r, and if the average interaction T is less than a critical value $T_C \approx W$, than no transport at all will be observed in the system [And58]. More precisely, he showed that under the above circumstances a single spin placed at one lattice site will remain exponentially localized even in the limit $t \to \infty$.

2.3 Localization in one Dimension

As the subject of this work are only one dimensional systems, we want to briefly review the known properties of Anderson localization in one dimension. General results on localization for arbitrary dimensions d have been found using scaling techniques. For a good review on this see [LR85] or chapter 8 in [She06]. By scaling arguments it was shown that for dimensions $d \leq 2$ all states are localized even for arbitrarily small disorder strength W, while for $d > 2$ a critical disorder strength exists, above which both localized and extended eigenstates might be found separated in energy by the mobility edge E_C. However, we want to restrict ourselves to one dimensional systems from now on.

2.3.1 Arguments from Random Matrix Theory

In this section, a simple one dimensional model will be introduced, where the localization of eigenfunctions can be derived from random matrix theory. This model is obtained from (2.2) by introducing nearest neighbor coupling: $T_{n,n+1} = T_{n,n-1} = A$. Note that the Hamiltonian is real and symmetric for this coupling and so the eigenstates are also real and we can treat a_n as real numbers. The equation for the eigenstates of such a system looks as follows:

$$\epsilon\, a_n = V_n a_n + A(a_{n-1} + a_{n+1}), \tag{2.3}$$

where ϵ is the eigenenergy of the eigenstate and the on-site energy is called V_n instead of E_i here. This can be written via transfer matrices T_n that describe the advance by one lattice site:

$$\begin{pmatrix} a_{n+1} \\ a_n \end{pmatrix} = T_n \begin{pmatrix} a_n \\ a_{n-1} \end{pmatrix}, \tag{2.4}$$

with the transfer matrix being defined as

$$T_n := \begin{pmatrix} (\epsilon - V_n)/A & -1 \\ 1 & 0 \end{pmatrix}. \tag{2.5}$$

Introducing the product Q_N of transfer matrices:

$$Q_N = \prod_{n=1}^{N} T_n, \tag{2.6}$$

equation (2.3) can be written in explicit form:

$$\begin{pmatrix} a_{N+1} \\ a_N \end{pmatrix} = Q_N \begin{pmatrix} a_1 \\ a_0 \end{pmatrix}. \tag{2.7}$$

It should be mentioned, that with this formulation one still has to find consistent combinations of ϵ, a_0 and a_1, fullfilling the boundary conditions, if one wants to solve (2.3). But suppose some sequence $\{a_n\}$ is a solution of (2.3), then (2.7) must be fulfilled for these a_n and theorems about products of random matrices can be applied.

The most interesting result about random matrices for our case is the Fürstenberg theorem which states the existence of the *maximal characteristic Lyapunov exponent* λ_1 for a sequence of products of random matrices P_n [CPV93]:

$$\lambda_1 = \lim_{N\to\infty} \frac{1}{N} \ln \parallel P_1 \cdot \ldots \cdot P_N \parallel, \tag{2.8}$$

where $\parallel \cdot \parallel$ denotes the ususal matrix/operator norm $||A|| = \max\{||Ax||\}$ where $||x|| = 1$. Moreover, λ_1 turns out to be nonrandom, thus independent of the actual choice of random matrices P_n. Fürstenberg also showed that for the case of uniformly distributed random matrices with determinant 1 (as the T_n are), λ_1 is always positive. Roughly spoken, this means that for some vector z we have

$$|Q_N z| \sim \mathrm{e}^{\lambda_1 \cdot N} |z|. \tag{2.9}$$

Applying this to eqn. (2.7), we see that the states a_n must be exponentially increasing with n, having an exponential growth rate $\lambda_1 > 0$. If we use the same lattice site as starting point and iterate to the other direction, we also see exponential growth in the system with the same rate λ_1. Now we assume periodic boundary conditions. That requires the iterations in both directions to match at some point if they belong to proper eigenstates. In general, those iterations will not match as the starting point a_0, a_1 or the chosen energy ϵ do not correspond to an eigenstate of the system. Anyhow, *if* an eigenstate for the chosen values of a_0, a_1 and ϵ does exist, it should be localized with localization lengths $\xi = 1/\lambda_1$. Furthermore, it is assumed that the behavior of λ_1 is sufficiently smooth so that a λ_1 found for some energy ϵ close to an eigenenery is also close to the inverse localization length of the corresponding eigenstate. This is called the Borland conjecture [Bor63]. See [CPV93] and references therein for more accurate mathematical treatments of this issue.

2.3.2 Density of States and Localization Length

Unfortunately, the energy dependence of the density of states (DOS) $\rho(E)$ and the localization length $\xi(E)$ can not be computed analytically for arbitrary disorders.[2] It should be noted first that $\rho(E)$ and $\xi(E)$ are understood as averages over many disorder realizations. However, from perturbation theory for weak disorders strengths (small W) follows that disorder destroys the divergence of ρ at the energy band edges that is seen in regular lattices. More precisely, the DOS has smooth exponential tails at the borders, called Lifshitz tails. We will not go into more details on that, but one important fact should be presented that can be obtained from a

[2] There exist exact results for Cauchy–distributed random disorder [Llo69].

Coherent Potential Approximation (CPA). The result was found by Thouless in 1974 [Tho74] and provides effective band edges for the eigenenergies. Following his calculations, the energy band edges are given by

$$|E_{\pm}| = \frac{1}{2}\sqrt{W^2 + 4A^2} + \frac{A}{W} \ln \frac{\sqrt{W^2 + 4A^2} + W}{\sqrt{W^2 + 4A^2} - W} \approx 2A + \frac{W^2}{12A}, \tag{2.10}$$

where the approximation is valid for small disorder strength W. Note that those edges are no sharp bounds. They rather mean that eigenenergies below (above) these edges occur with exponentially small probability.

For the localization length $\xi(E)$, second order perturbation theory for weak disorder strength W in the 1D Anderson system (2.3) gives the following dependence ($|E| < 2A$):

$$\xi(E) = \frac{96A^2 - 24E^2}{W^2} \tag{2.11}$$

Remember, that A is the coupling strength of nearest-neighbor coupling and W the strength of disorder.

Nevertheless, the formulation with transfer matrices (2.4) is an useful tool for numerical studies on $\rho(E)$ and $\xi(E)$. To evaluate the density of states, we have to know that in one dimensional systems the eigenstates can be labeled by ascending energy. Say a_n^k are the values of the k-th eigenstate of our system at lattice site n, where $k = 0$ corresponds to the state of lowest energy. Now for one dimensional systems, we also know that the k-th eigenstate must have precisely k nodes, which means zero crossings [PF92], neglecting degenerated cases. Additionally, the number of states below the energy given by the k-th eigenenergy is precisely k. Thus, given a lattice of size N we can compute the integrated density of states for the eigenenergies as

$$\eta(\epsilon_k) := \int_{-\infty}^{\epsilon_k} \mathrm{d}E' \rho(E') = \frac{k}{N}. \tag{2.12}$$

Together with the Borland conjecture, this leads to an easy applicable numerical method for computing the integrated density of states η. The straightforward way would be to fix some initial conditions and iterate the mapping (2.4) for different energies ϵ. To obtain the number zero crossings k and hence $\eta(\epsilon_k)$, one simply counts the points where a_n changes its sign. But as a_n is exponentially increasing with n, one might not be able to iterate long enough to get a sufficiently exact approximation due to the limited maximal numbers that can be handled by a computer.

This can be overcome by using a slightly transformed mapping. Therefore, new variables R_n are introduced, defined by

$$R_n := a_{n+1}/a_n. \tag{2.13}$$

For R_n, the equation for an eigenstate of the system leads to the following iteration map:

$$R_{n+1} = E - V_n - \frac{1}{R_n}. \tag{2.14}$$

Note, that the coupling strength A is set to 1 for sake of simplicity. Using this iteration overcomes the problem of exponential growth, and by counting the negative values of R_n

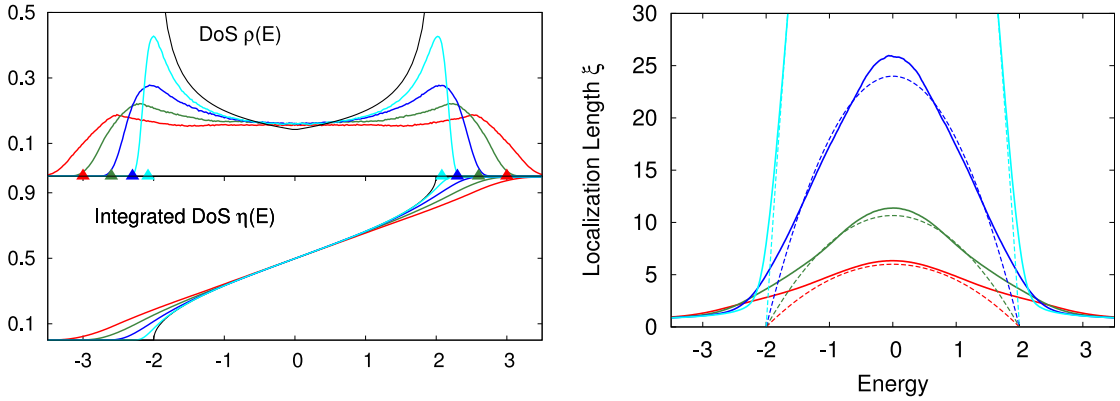

Figure 2.1: Density of states $\rho(E)$ (top left), integrated DOS $\eta(E) = \int \rho(E)$ (bottom left) and localizations length $\xi(E)$ (right) for different disorder strengths $W = 1.0$ (light blue), $W = 2.0$ (blue), $W = 3.0$ (green) and $W = 4.0$ (red). Coupling constant $A = 1$. Numerical results were obtained by iterating (2.14) 10000 steps for 1000 disorder realizations. The black curves in the left plots shows the diverging behavior of the DOS $\rho(E) \sim 1/\sqrt{2 - |E|}$ near the spectrum borders $E_\pm = \pm 2$ for the regular lattice ($W = 0$) for comparison. The small triangles mark the effective energy edges as given by equation (2.10). The localization lengths for different disorders are plotted on the right. The colors are the same as in the left plot. The dotted lines are the approximations from (2.11).

one gets the number of nodes of a_n and thus the integrated density of states for a given energy E. Moreover, the average of the values $\ln |R_n|$ gives an approximation for the localization length $\xi(E)$. Obviously, those values still depend on the disorder realization that was chosen for the iteration, but not on the initial values a_0 and a_1, at least for large numbers of iterations N. Therefore, an averaging over disorder realizations should also be applied to obtain universal, non-random results. Hence, the following quantities are computed from iterating (2.14):

$$\eta(E) = \left\langle \frac{1}{N} \sum_{n=1}^{N} \theta(R_n) \right\rangle_\Omega \tag{2.15}$$

$$\xi(E) = \left\langle \frac{1}{N} \sum_{n=1}^{N} \ln |R_n| \right\rangle_\Omega , \tag{2.16}$$

where θ is the usual step function and $\langle \cdot \rangle_\Omega$ denotes the averaging over disorder realizations, that is, sets of random potential values V_n. Fig. 2.1 shows numerical results for $N = 10,000$ averaged over $1,000$ disorder realizations. For increasing disorder strength $W > 0$, one sees the Lifshitz tails at the edges of the energy band, whereas for the regular lattice the density of states $\rho(E) = \mathrm{d}\eta/\mathrm{d}E$ is diverging at those points. For large disorder strength $W = 4$, $\eta(E)$ is nearly linear for almost the whole energy band, which means a roughly constant density $\rho(E)$. The localization length ξ has its maximum at the center of the energy band $E \approx 0$ and is also increasing for decreasing disorder strength W. This is expected, as ξ should diverge for $W \to 0$. In the right panel in Fig. 2.1, the numerical results for $\xi(E)$ are compared with the approximations from (2.10) showing a good correspondence for energies away from the band edges.

2.3.3 Localization and Conductivity

In this section, the relation between conductivity (diffusion) and localization is going to be enlightened by showing that for a 1D disordered system the conductivity will vanish. We start with the Landauer formula [Lan70] which states that for an electronic system the conductivity G through some (1D) probe is proportional to the quotient of transmission coefficient T and diffusion coefficient R of this probe:

$$G \sim \frac{T}{R} \tag{2.17}$$

The probe itself is considered as a random one dimensional system with N lattice sites. Left and right of the probe, we assume free electrons with wave number k and thus write the wavefunctions there as:

$$\text{left}: \ \psi_n = \mathrm{e}^{ikn} + r\mathrm{e}^{-ikn} \ (n \leq 0) \tag{2.18}$$

$$\text{right}: \ \psi_n = t\mathrm{e}^{ikn} \ (n > N), \tag{2.19}$$

where we suppose the incident wave coming from the left. t and r are the complex transmission/reflexion coefficients with $R = |r|^2$ and $T = |t|^2$. Those wavefunctions can be related using the product Q_N of transfer matrices from eq. (2.7):

$$\begin{pmatrix} t\mathrm{e}^{ikN} \\ t\mathrm{e}^{ik(N-1)} \end{pmatrix} = Q_N \begin{pmatrix} 1+r \\ \mathrm{e}^{-ik} + r\mathrm{e}^{ik} \end{pmatrix}. \tag{2.20}$$

This can be solved for t, yielding [CPV93]:

$$|t| = \frac{2|\sin k|}{|(Q_N)_{21} - (Q_N)_{12} + (Q_N)_{22}\mathrm{e}^{ik} - (Q_N)_{11}\mathrm{e}^{-ik}|}. \tag{2.21}$$

Applying the Fürstenberg theorem, we find

$$G \sim |t|^2 \sim \mathrm{e}^{-2\lambda_1 N} \sim \mathrm{e}^{-N/\xi}. \tag{2.22}$$

This holds because for non strictly positive matrices, like the transfer matrices T_n (2.4), it can be shown that not all components of the product matrix Q_N are growing with an exponential rate λ_1. Thus, the denominator in (2.21) does not vanish, but increases like $\mathrm{e}^{\lambda_1 N}$. Hence, we found exponentially decaying conductance for an one dimensional system with disorder.

3 Discrete Nonlinear Schrödinger Equation

3.1 DNLS and its history

The Discrete Nonlinear Schrödinger equation (DNLS) in its simplest interpretation describes a chain of coupled, anharmonic, classical oscillators in one spatial dimension. Mathematically, it is described by the following set of equations of motion:

$$i\frac{\mathrm{d}}{\mathrm{d}t}\psi_j = A(\psi_{j+1} + \psi_{j-1}) + \beta|\psi_j|^2\psi_j, \tag{3.1}$$

where i is the imaginary unit and j is the lattice index. ψ_j can be considered as the complex mode amplitude of the oscillator at site j and A is the nearest neighbor coupling strength while β is the nonlinear strength. The typical oscillator term $\sim k\psi_i$ on the rhs. of 3.1 disappears under a simple transformation and is usually neglected for coupled systems as is shown in section 3.2.1. In numerical studies, the lattice is considered finite, i. e. $j = 1 \dots N$, and usually periodic boundary conditions are applied, i. e. $\psi_{j+N} = \psi_j$. The DNLS can be considered as a special case of a so called Discrete Self-Trapping (DST) equation:

$$i\frac{\mathrm{d}}{\mathrm{d}t}\psi_j = \sum_k A_{jk}\psi_k + \beta|\psi_j|^2\psi_j, \tag{3.2}$$

where $A = [A_{jk}]$ is the $N \times N$ coupling matrix, which is usually symmetric in physical systems. Choosing A tridiagonal, one again gets (3.1) where diagonal terms $A_{jj}\psi_j$ can be neglected as said before.

For the nearest neighbor coupling (3.1), the number of parameters can be decreased by dividing the equation by A and using the transformation $t \mapsto At$, $\beta \mapsto \beta/A$ resulting in

$$i\frac{\mathrm{d}}{\mathrm{d}t}\psi_j = \psi_{j+1} + \psi_{j-1} + \beta|\psi_j|^2\psi_j, \tag{3.3}$$

which from now on is called *the* DNLS equation.

There already exist over 350 papers concerning DNLS or DST equations dealing with all kinds of effects in those systems, for example: wave transmission [HT99], localized modes and their stability [PGK01] or breather solutions [KA00]. For a review on the major results and historical aspects see also [EJ03].

3.2 Sources of the DNLS

3.2.1 Discretization of the Nonlinear Schrödinger Equation

Besides the interpretation as a system of coupled oscillators, the easiest way to obtain the DNLS is from a straightforward discretization of the Nonlinear Schrödinger equation (NLS)

$$i\hbar\frac{\partial\phi}{\partial t} = -\frac{1}{2m}\frac{\partial^2\phi}{\partial x^2} + \gamma|\phi|^2\phi \left(= \hat{H}\phi\right) \tag{3.4}$$

by a spatial discretization $\phi(x) \to \phi_j = \phi(x_j)$ where $x_j = x_0 + j \cdot \Delta x$. The spatial derivative then is approximated by a finite difference

$$\left.\frac{\partial^2 \phi}{\partial x^2}\right|_{x_j} \longrightarrow \frac{1}{(\Delta x)^2}(\phi_{j-1} - 2\phi_j + \phi_{j+1}). \tag{3.5}$$

By applying the following transformations

$$\begin{aligned} \phi_j \mapsto \psi_j &:= \phi_j \mathrm{e}^{2i\hbar t/2m(\Delta x)^2} \\ t \mapsto \tau &:= -\hbar t/m(\Delta x)^2 \\ \gamma \mapsto \beta &:= -(\Delta x)^2 \gamma \end{aligned}$$

we get, denoting the derivative with respect to the new time τ by a dot,

$$i\dot{\psi}_j = \psi_{j-1} + \psi_{j+1} + \beta|\psi_j|^2\psi_j \tag{3.6}$$

which is exactly (3.3). By this transformation, the term $2\phi_j$ disappeared and in the same way any term $k\phi_j$ can be neglected as the system can always be transformed to a rotating frame where this term vanishes.

It is worth pointing out that there are other possible discretizations of (3.4), one of which being the Abowitz–Ladik (AL) model:

$$i\frac{\mathrm{d}}{\mathrm{d}t}\psi_j + \left(1 + \frac{1}{2}\gamma|\psi_j|^2\right)(\psi_{j+1} + \psi_{j-1}) = 0. \tag{3.7}$$

The AL model, in contrast to the DNLS, is fully integrable, but it can be argued that it is physically less meaningful.

3.2.2 Interacting Bose-Einstein Condensates

It is well known that the dynamics of a weakly interacting Bose gas at zero temperature in a harmonic trap can be described by the Gross-Pitaevskii equation, which is the same as the NLS (3.4) plus an external potential [DGPS99]. Starting from a 1D many body Hamiltonian in second quantization, the DNLS is going to be derived using mean field approximation techniques for a Bose-Einstein condensate. We follow the calculations presented in [MC08] starting with the Hamiltonian:

$$\begin{aligned} \hat{H} = &\int \mathrm{d}x\, \hat{\psi}^\dagger(x) \left[-\frac{\hbar^2}{2m}\frac{\partial^2}{\partial x^2} + V_{\mathrm{ext}}(x)\right] \hat{\psi}(x) \\ &+ \frac{1}{2}\int \mathrm{d}x \int \mathrm{d}x'\, \hat{\psi}^\dagger(x') V_{\mathrm{int}}(x - x')\hat{\psi}(x')\hat{\psi}(x). \end{aligned} \tag{3.8}$$

$\hat{\psi}^\dagger(x)$ and $\hat{\psi}(x)$ are the bosonic field operators which destroy/create a particle at position x. Those can be expanded into localized[1] Wannier functions $\hat{\psi}(x) = \sum_j \hat{b}_j w(x - x_j)$, where $\hat{b}_j$ destroys a particle in the Wannier wavefunction $w(x - x_j)$. Additionally, the interaction

[1] Assuming that the potential is strong enough, we can invoke the tight-binding approximation for which the Wannier functions are understood to be localized.

potential V_{int} is assumed to be of contact type, namely $V_{\text{int}}(x - x_j) = g\delta(x - x_j)$, where g is roughly the s-wave-scattering length of atoms. Under those assumptions, (3.8) can be approximated by keeping only nearest neighbor hoppings and on-site interactions and we arrive at the so called Bose-Hubbard-Hamiltonian (BHH):

$$\hat{H} = -J \sum_{j=1}^{N-1} (\hat{b}_{j+1}^{\dagger} \hat{b}_j + \text{h.c.}) + \frac{U}{2} \sum_{i=j}^{N} \hat{n}_j (\hat{n}_j - \mathbb{1}) + \sum_{j=1}^{N} V_j \hat{n}_j. \tag{3.9}$$

$\hat{n}_j \equiv \hat{b}_j^{\dagger} b_j$ is the number operator counting the number of bosons in the Wannier function at lattice site j. The coefficients J, U and V_j can be computed exactly in terms of the single particle wavefunctions $w(x - x_j)$ [JBC+98]. However, their meaning can be seen from (3.9). J is the nearest neighbor hopping coefficient, U the on-site interaction energy and V_j represents the external potential. The DNLS can be recovered from the BHH simply by applying the time evolution in the Heisenberg picture $i\hbar\partial_t \hat{b}_k = [\hat{b}_k, \hat{H}]$. After some straight forward computation using commutator relations for the creation/annihilation operators, one arrives at

$$i\hbar\partial_t \hat{b}_k = -J(\hat{b}_{k+1} + \hat{b}_{k-1}) + U\hat{b}_k \hat{b}_k^{\dagger} \hat{b}_k + V_k \hat{b}_k. \tag{3.10}$$

That is already the DNLS plus the potential term V_k, but rather for operators $\hat{b}_k$ than for wavefunction amplitudes. Using the expectation value of eq. (3.10), an equation for the expectation value $\langle \hat{b}_k \rangle =: \chi_k$ can be obtained that is precisely the DNLS plus potential term.

$$i\hbar\partial_t \chi_k = -J(\chi_{k+1} + \chi_{k-1}) + U|\chi_k|^2 \chi_k + V_k \chi_k. \tag{3.11}$$

3.2.3 Coupled Optical Waveguides

To underline the wide applicability of the DNLS, we want to present an occurrence away from BCEs or the solid state context. The example will be a system of coupled optical waveguides, but only a brief overview on how the DNLS is obtained will be given, as the complete mathematical derivation is beyond the scope of this text. For a detailed treatment see [HT99]. Consider a system of coupled, nonlinear, optical waveguides that are extended in z-direction. Denoting the amplitude of the μ-th normal mode of the n-th waveguide by $a_{\mu,n}$, we can write down the following relation:

$$-i\frac{\mathrm{d}}{\mathrm{d}z} a_{\mu,n} \sim \int \mathrm{d}x\mathrm{d}y E_{\mu,n} \cdot P'_n, \tag{3.12}$$

where $E_{\mu,n}$ is the electric field of the μ-th mode in the n-th waveguide and P' is the polarization induced by surrounding waveguides and nonlinear material effects. Depending on the material and its dielectric coefficients, magnetic susceptibility and nonlinear properties, there might appear many kinds of terms in P'. Using coupled nonlinear waveguides, the polarization has a form that already reminds of the DNLS:

$$P'_n = \epsilon_1 E_n + \epsilon_2 (E_{n-1} + E_{n+1}) + \chi |E_n|^2 E_n. \tag{3.13}$$

ϵ_1 and ϵ_2 are dielectric constants of the waveguide and the surrounding host material respectively. χ is the nonlinear magnetic susceptibility and E_n denotes the total electric field from the n-th waveguide. By making the simplification that only the lowest mode contributes

to the field, namely $E_n \sim a_{\mu=1,n}$, one arrives, after some integration, at an equation for amplitudes of the first modes $a_n \equiv a_{\mu=1,n}$:

$$-i\frac{\mathrm{d}}{\mathrm{d}z}a_n = Q_n a_n + \widetilde{Q}_{n,n-1}a_{n-1} + \widetilde{Q}_{n,n+1}a_{n+1} + \widehat{Q}_n|a_n|^2 a_n, \tag{3.14}$$

where $Q, \widetilde{Q}$ and $\widehat{Q}$ are the integrals over different orders of E as given by substituting (3.13) into (3.12). If identical waveguides are used, the coupling coefficients $\widetilde{Q}$ become real and symmetric and after a phase transformation $a_n = c_n \exp(iQ_n z)$ we arrive at:

$$i\frac{\mathrm{d}}{\mathrm{d}z}c_n = V(c_{n-1} + c_{n+1}) - \gamma|c_n|^2 c_n, \tag{3.15}$$

where $-V := \widetilde{Q}_{n,n-1} = \tilde{Q}_{n,n+1}$ and $\gamma = \widehat{Q}_n$ was introduced. This, again, is the DNLS, but instead of the time evolution of a solid state system, it describes the behavior of the electromagnetic field in optical waveguides. So what usually was the time derivative in the former examples is now replaced by a spatial derivative corresponding to the direction along the waveguide.

Optical waveguides provide a very good experimental access to disordered, nonlinear systems where most of the parameters can be controlled quite precisely in the experimental setup.

3.3 Properties of the DNLS

3.3.1 Conserved Quantities

Before advancing to disordered lattices, a few properties of the DNLS will be reviewed. Maybe the most interesting ones are the conserved quantities, as they have huge impacts on the dynamics of the system. As a matter of fact, there are precisely two conserved quantities for the DNLS: the norm $\mathcal{N}$, usually set to 1:

$$\mathcal{N} = \sum_{j=1}^{N} \psi_j^* \psi_j = 1 \tag{3.16}$$

and the energy E

$$E = \sum_{j=1}^{N} A(\psi_{j+1}^* \psi_j + \psi_{j+1}\psi_j^*) + \frac{\beta}{2}|\psi_j|^4 \tag{3.17}$$

It is obvious, just from the origin of the DNLS equation, that both of these quantities must be conserved. Their validity can also be quickly seen by computing the time derivative of (3.16), (3.17) respectively, and substituting the DNLS (3.3) and its complex conjugate. As said before, these are the *only* conserved quantities [EJ03]. Thus, the DNLS is not integrable for $N > 2$.

3.3.2 Traveling Wave Solutions

Using the ansatz describing a traveling wave with frequency ω

$$\psi_n(t) = R\,\mathrm{e}^{i(kn-\omega t)} \tag{3.18}$$

to solve the DNLS (3.3), we find the dispersion relation

$$2\cos k = \omega - \beta|R|^2. \tag{3.19}$$

k must be real valued for the solution (3.18) to be of physical meaning. This restricts the frequency, and thus the energy, of the wave to the band

$$-2 + \beta|R|^2 < \omega < 2 + \beta|R|^2. \tag{3.20}$$

Compared with the linear case $\beta = 0$, we see that the nonlinearity simply shifts the energy band.

3.3.3 Breather Solutions

Breathers are very interesting objects in nonlinear systems. However, they are not the major effects that are considered in this work, but they will be used to explain some observations in the later parts, so a few words about these structures are necessary. For a detailed review on breathers in discrete systems see [Aub97], for example.

Breathers are usually understood as time periodic (or quasi periodic), spatially localized solutions of nonlinear systems. They appeared first in the context of the *sine-Gordon PDE*: $u_{xx} - u_{tt} = \sin u$. Note that these objects are of completely different nature than the localized eigenmodes of the linear Anderson model. Breathers are inherently nonlinear phenomena – the breather solution (in general) does not solve the linearized equations of the underlying nonlinear system. They have, however, in common that breathers as well as Anderson modes exhibit no dissipation even for $t \to \infty$. In 1994, MacKay and Aubry presented a proof showing the existence of infinitely many breathers in systems of weakly coupled, nonlinear oscillators [MA94]. The idea of the proof is to continue the solution of an uncoupled system, which is fully integrable, to the case of small but non-vanishing coupling. The case without coupling is called the *anti-continuous-limit*. For uncoupled oscillators it is obvious that by exciting one oscillator, having the frequency ω, and leaving the others at rest, we have a time periodic solution of the system. It can now be shown that this solution can be continued for increasing coupling up to some critical value at which some sort of bifurcation appears and the breather is destroyed. The oscillation frequency remains constant during the continuation process and it can also be shown that the continued solution is exponentially localized.[2]

[2]Note that the original solution is a delta-peak and thus as localized as possible.

4 Discrete Anderson Nonlinear Schrödinger Equation

4.1 The gDANSE Model

After having introduced systems with disorder in chapter 2 and a nonlinear system in chapter 3, the actual model investigated in the later parts of this work will be presented. The underlying equation is a combination of the two former and is usually referred to as the *Discrete Anderson Nonlinear Schrödinger Equation* (DANSE):

$$i\frac{\mathrm{d}}{\mathrm{d}t}\psi_n = V_n\psi_n + \psi_{n-1} + \psi_{n+1} + \beta|\psi_n|^2\psi_n. \tag{4.1}$$

As before, ψ_n is the complex valued oscillator state at site n and V_n is the on-site potential, chosen uniformly random from the interval $[-W/2, W/2]$. This choice of the random potential has, in the limit $N \to \infty$, a mean value of zero $\overline{V} = \sum V_n/N \to 0$ what seems somehow special. But suppose we have some random distribution V_n' with mean $\overline{V}' \neq 0$, then by taking $V_n = V_n' - \overline{V}'$ and using the transformation $\psi_n \mapsto \psi_n \exp(-i\overline{V}'t)$ the above equation is re-established. Thus, the mean value of the random potential is arbitrary and we choose the disorder such that its mean will be zero in the limit for large N. β gives the strength of the nonlinear term and is mostly set to 1 in this work. The state given by the sequence of complex numbers $\psi = (\psi_n)$ will sometimes be called wavefunction as well, due to the correspondence with the Schrödinger equation.

However, in part II a somewhat academical generalization of (4.1) is considered:

$$i\frac{\mathrm{d}}{\mathrm{d}t}\psi_n = V_n\psi_n + \psi_{n-1} + \psi_{n+1} + \beta|\psi_n|^{2\alpha}\psi_n. \tag{4.2}$$

The meaning of the symbols is:

$n = 1 \dots N$	spatial lattice index
$\psi_n \in \mathbb{C}$	oscillator state at lattice site n
$V_n \in [-W/2, W/2]$	random potential, distributed uniformly
$\beta \in \mathbb{R}$	nonlinear strength, usually 1.0
$\alpha = 0.5, 1, 2, 3$	nonlinearity index

A new parameter α is introduced that describes the shape of the nonlinear potential and will be called *nonlinearity index*. $\alpha = 1$ corresponds to the original DANSE. Note that due to the condition $|\psi_n| < 1$, larger values of α decrease the influence of nonlinearity, while for smaller α the nonlinear effects are increased. Eq. (4.2) is called *generalized DANSE (gDANSE)* from now on and we usually set $\beta = 1$ and only α is varied. The corresponding Hamiltonian has the form

$$\mathcal{H} = \sum_n V_n|\psi_n|^2 + \psi_{n-1}\psi_n^* + \psi_n\psi_{n-1}^* + \frac{\beta}{\alpha+1}|\psi_n|^{2(\alpha+1)}. \tag{4.3}$$

Thus, we again have norm and energy conservation in our system.

4.2 Eigenmode Representation

Later, we will often refer to the DANSE or gDANSE in another form that is very helpful to understand some of the observations. This representation can be obtained by a simple base transformation from the spatial peaks ψ_n to eigenmodes ϕ_m of the linear part of the DANSE. This linear part is nothing else than the Anderson model (2.2). We introduce new variables C_m that represent the excitation strengths of the m-th linear mode ϕ_m. The relation to the old spatial variable ψ_n is:

$$\psi_n = \sum_m C_m \phi_{m,n} \tag{4.4}$$

where $\phi_{m,n}$ is the, in general complex, value of the m-th eigenfunction at lattice site n. As the Hamiltonian of our system is usually real and symmetric, the eigenfunctions are always real valued as well. The calculations are, however, done for the general case of complex valued eigenfunctions. Using the decomposition above and the fact that the ϕ_m are eigenmodes of the linear part with eigenvalues ϵ_m, (4.2) can be transformed to an equation describing the time dependence of the new variables C_m:

$$i\frac{\mathrm{d}}{\mathrm{d}t}C_m = \epsilon_m C_m + \beta \sum_{\substack{\widehat{m}_1 \dots \widehat{m}_\alpha \\ \widetilde{m}_1 \dots \widetilde{m}_\alpha \\ m'}} V^{\widehat{m}_1 \dots \widehat{m}_\alpha}_{\widetilde{m}_1 \dots \widetilde{m}_\alpha \; m',m} C_{\widehat{m}_1} \cdots C_{\widehat{m}_\alpha} C^*_{\widetilde{m}_1} \cdots C^*_{\widetilde{m}_\alpha} C_{m'}. \tag{4.5}$$

The sum is taken over $2\alpha + 1$ indices $\widehat{m}_1, \widehat{m}_2 \dots \widehat{m}_\alpha$, $\widetilde{m}_1, \widetilde{m}_2 \dots \widetilde{m}_\alpha$ and m'. The coupling in this representation is nonlinear and governed by the eigenmode overlaps V. For a rigorous derivation of this equation and the exact definition of V see appendix A.1. If α is set to 1, the summation has to be done only over three indices $\widehat{m}, \widetilde{m}, m'$ and the coupling strength is the four-eigenmode-overlap $V_{\widehat{m},\widetilde{m},m',m}$.

4.3 Properties of the DANSE

4.3.1 Breathers

In section 3.3.3 it was argued that there exist time periodic, localized solutions in the regular[1] nonlinear system. The existence of such structures in the presence of disorder has been addressed in much detail by Kopidakis and Aubry in 1999 [KA99a, KA99b] and their results should be mentioned here. First of all, in the limit of vanishing coupling it is obvious that single excited nonlinear oscillators still give a localized time-periodic solution of the problem. Those solutions can be continued for small coupling, if the frequency is, and remains, *outside the linear spectrum*. These solutions are called extraband discrete breathers (EDB). If, however, the frequency of such a breather enters the phonon spectrum during the continuation[2], bifurcations occur and the breather disappears [KA99a]. Thus, the techniques used to find breathers in the DNLS is not successful if disorder is introduced – disorder destroys the localization effects of nonlinearity, except for solutions outside the phonon spectrum where the nonlinearity is so strong that the influence of disorder is negligible.

[1] "regular" means without disorder.

[2] Mind, that by increasing the coupling, the spectrum of the linear eigenenergies gets broader and eventually reaches the frequency of the breather.

But there is another approach that turned out to be more successful [KA99b]. The technique is slightly different from the one above, but the idea is similar: One takes the localized eigenmodes of the linear problem and tries to continue them for increasing nonlinearity. It is convenient to use the eigenmode representation of the DANSE equation, where the nonlinear term is now being found in the coupling. Starting with eigenmodes at zero nonlinear coupling one can (sometimes) safely continue the localized solution for increasing coupling up to some critical value, were eventually a bifurcation destroys the solution. Using this method, Aubry and Kopidakis found linearly stable, exponentially localized breathers emerging from the eigenmodes of the linear system for small nonlinearities. There are, of course, some restrictions on the frequencies of these modes, but we refer to [KA99b] for any details on this. However, the important fact is that these localized solutions do exist and this is used to explain some of the numerical results found in part III and also provides some arguments for the next section.

4.3.2 Spreading Regimes

The best way to understand why localized states spread in the DANSE model is to consider the interactions between the localized eigenmodes of the linear equations. Without nonlinearity ($\beta = 0$), eigenmodes with corresponding eigenvalues ϵ_m of the system can be easily calculated. All eigenmodes are exponentially localized due to Anderson localization and the eigenenergies (or frequencies) ϵ_m are random[3] and lie within an interval of width $\Delta \lesssim W + 4$.

Qualitatively, three regimes of nonlinear strength with different spreading behavior can be expected:

Weak Nonlinearity: The nonlinear strength β is small so that continued breather solutions still exist and no spreading is expected.

Moderate Nonlinearity: The breather solution has bifurcated and the nonlinearity might cause spreading of initially localized states in the system.

Strong Nonlinearity: The nonlinear strength is so strong that the total energy of the states is shifted out of the linear spectrum. That creates extra-band breathers (EBD) that also cannot spread [KA99a].

The different regimes were also addressed by some calculations from Flach et al. [FKS09] which are briefly reviewed here: If the disorder strength is large enough, $W \gtrsim 3$, the density of states is approximately constant, as is shown in section 2.3.2, and the average distance between the eigenvalues can be approximated by Δ/N, where N is the lattice size – number of eigenmodes respectively. The localization length $\xi(\epsilon_m)$ of the eigenmodes has its maximum value at the band center $\epsilon_m = 0$ given by $\xi(0) \approx 100/W^2$ (section 2.3.2). An exponentially localized state has a Participation Number[4] of $P(\epsilon_m) \lesssim 4\,\xi$, as is shown in section 5.1. Taking the Participation Number as spatial extend of the wavefunction, we find about $P(\epsilon_m)$ eigenmodes within the region of eigenmode m. Then, a rough approximation of the mean distance of eigenenergies is:

$$\overline{\Delta\epsilon} \approx \frac{\Delta}{P(\epsilon_m)} \overset{W=4.0}{\approx} \frac{(4+W)W^2}{4 \cdot 100} \approx 0.3. \tag{4.6}$$

[3] The probability distribution of the eigenenergies is nontrivial and depends on W.
[4] The Participation Number measures the extend of a distribution – details will be presented in chapter 5.

Now for $\beta > 0$, the nonlinear terms cause an energy shift of order β to the eigenmodes due to the nonlinear coupling. Furthermore, the coupling strength decreases exponentially with spatial distances of the eigenmodes and so we say that only the modes within a region of size $P(\epsilon_m)$ are effectively excitable. This again gives the three regimes of nonlinearity from above: $\beta < \overline{\Delta\epsilon}$ represents the weak nonlinearity where the local energy shifts are too small to cause spreading. $\overline{\Delta\epsilon} < \beta < \Delta$ is the intermediate regime where spreading is expected, and $\Delta < \beta$ coincides with the strong nonlinearity where the state energy is shifted out of the linear energy band and no spreading should occur.

These considerations are, however, rather a hypothesis and not a proof and should be checked in more detail in later works. Furthermore, Eq. (4.6) gives only a very rough estimate for the critical β at which spreading should start. Moreover, those values are averages and subject to strong fluctuation depending on the actual eigenmode in question and its vicinity. Note also that choosing states with energies close to the band edges leads to initially excited eigenmodes with very small localization lengths. According to the calculations above this increases the critical value of β, maybe even to values larger than 1.

4.4 Numerical Time Evolution

The numerical results in the later parts of this work are mainly obtained by applying a time evolution to some initial state according to the (g)DANSE equation. Due to the fact that the system is not integrable, one has to rely on numerical methods. This can be done by a discretization of time and evolving small timesteps linearly. In the following, the algorithm used throughout this thesis is introduced, where we provide calculations for the DANSE equation, but the generalization to the gDANSE is obvious. We start with writing the time dependent wavefunction $\psi_n(t)$ as a time evolution of some initial state $\psi_n(0)$ in terms of the time evolution operator $\hat{U}$.

$$\psi_n(t) = \hat{U}(t)\psi_n(0). \tag{4.7}$$

If we substitute this into (4.1), we find a operator equation for the time evolution operator U:

$$i\frac{\mathrm{d}}{\mathrm{d}t}\hat{U}(t) = \hat{H}\hat{U}(t), \tag{4.8}$$

which has the formal solution

$$\hat{U}(t) = \mathrm{e}^{-i\hat{H}\cdot t}. \tag{4.9}$$

To be able to construct an integration algorithm, we have to split $\hat{H}$ into two parts:

$$\hat{H} = \hat{H}_0 + \hat{B} \tag{4.10}$$

$$\hat{H}_0\psi_n = \psi_{n+1} + \psi_{n-1} + V_n\psi_n \tag{4.11}$$

$$\hat{B}\psi_n = \beta|\psi_n|^2\psi_n, \tag{4.12}$$

the linear part $\hat{H}_0$ and the nonlinear part $\hat{B}$. Note, for mathematical exactness, that the operator $\hat{H}_0$ acts on the whole wavefunction $\psi = (\psi_n)$ and the above equation should be understood in the meaning $\hat{H}_0\psi_n = (\hat{H}_0\psi)_n$ and similar for the other operators. If we use the splitting together with eq. (4.9), we find the following expression for $\hat{U}$:

$$\hat{U}(t) = \mathrm{e}^{-i(\hat{H}_0+\hat{B})\cdot t} \approx \mathrm{e}^{-i\hat{B}t}\cdot\mathrm{e}^{-i\hat{H}_0 t}. \tag{4.13}$$

The last step is an approximation because $\hat{H}_0$ and $\hat{B}$ are not commuting and therefore we make an error of order $|\hat{H}_0| \cdot |\hat{B}| \cdot t^2$ by this splitting. But the splitting is unitary and thus the total probability is preserved by this approximation [LR05].

To keep the error from the operator splitting sufficiently small, we integrate only over small timesteps $\Delta t = 0.1$. The time evolution for each such timestep can be written as:

$$\psi_n(t + \Delta t) = \mathrm{e}^{-i\hat{B}\Delta t}\mathrm{e}^{-i\hat{H}_0\Delta t}\psi_n(t). \tag{4.14}$$

From (4.12), we see that the nonlinear timestep is a simple matrix multiplication of ψ by a diagonal matrix with values $\exp(-i\beta|\psi_n|^2)$ as diagonal elements. The linear timestep is non-trivial and another approximation has to be used for solving the time evolution: The *Crank-Nicolson Scheme* [PTVF02]. Basically, it cuts down to an approximation of the exponential function

$$\mathrm{e}^{-i\hat{H}_0\Delta t} \approx \frac{1 - i\hat{H}_0\Delta t/2}{1 + i\hat{H}_0\Delta t/2} \tag{4.15}$$

which is accurate to second order in time and, again, unitary, thus norm preserving. If we denote the wavefunction after one *linear* timestep with $\tilde{\psi}$, we get the following relation:

$$(1 + i\hat{H}_0\Delta t/2)\tilde{\psi} = (1 - i\hat{H}_0\Delta t/2)\psi. \tag{4.16}$$

Considering the linearity of $\hat{H}_0$, we see that this is actually a set of linear equations that can be solved with numerical effort of order N (system size), due to the band structure of $\hat{H}_0$.

There exist other techniques for the numerical time-evolution, two of which should also be mentioned. If one uses a slightly different operator splitting by defining the linear part as $\hat{H}_0\psi_n = \psi_{n-1} + \psi_{n+1}$ and adding the diagonal disorder term to the nonlinear part, one can do the linear time step in terms of a *Fourier Transform*. This technique is remarkably faster than the Crank-Nicolson scheme (up to 30% in our tests), but has two downfalls. First, starting with a delta peak and doing a for- and backward-transformation we end up with all sites being weakly excited ($\sim 10^{-16}$) due to the finite Fourier transform. This could unintentionally support the spreading of wavefunctions just as a numerical effect. Secondly, by adding the linear potential term to the nonlinear part in the operator splitting, this nonlinear part does not decrease to zero for increasing spreading of the wavefunction. If the nonlinear part is only given by $|\psi_n|^2$, norm conservation ensures that it decreases if the wavefunction gets broader. However, an additional term V_n prevents that. Now the error done by the operator splitting is $\sim [\hat{H}_0, \hat{B}]$ and hence vanishes if $\hat{B} \to 0$, which is not happening with the Fourier method.

The first problem can be overcome by the usage of *Bessel-Functions* instead of Fourier transforms. However, this method is clearly slower than our Crank-Nicolson scheme and still has the disadvantage of lesser accuracy for broader states. Thus, in our opinion the Crank-Nicolson algorithm is the best choice for numerical integration of the DANSE equation.

Part II

Subdiffusive Spreading

In this part mainly, the spreading behavior of initially localized states in large disordered nonlinear lattices is investigated. The fundamental question is whether or not nonlinearity destroys Anderson localization. Many, partly contradicting results have been published on this topic already.
Firstly, the methods for measuring the degree of localization of wavefunctions or probability distributions are described and a new tool, the *structural entropy*, is introduced. This new value allows for the investigation of the peak structure of states and it is used to check the time dependence of the peak structure of spreading wavefunctions. Furthermore, a generalization to the usual DANSE system is considered introducing nonlinear indices (see section 4.1). Finally, the spreading behavior in such a system is discussed analytically and the obtained results are compared with numerical simulations.

5 Measures of Localization

There exist a few different approaches to determine whether a probability distribution is localized or not. The most straightforward one would be to simply fit an exponential decay and use the fitted localization length. Obviously, this requires high numerical effort and produces rather poor results when significant noise is present, like in the Anderson model. Former works on this problem mainly used the second moment $(\Delta x)^2 = \langle x^2 \rangle - \langle x \rangle^2$ of the wavefunction or the inverse Participation Number $P^{-1} = \sum |\psi_n|^4$ to measure the localization of a distribution. Our new approach will be to additionally use a generalization of the Participation Number according to generalized Rényi entropies. This will allow us not only to investigate the spreading of the wavefunction, but as well provides a tool to analyze its peak structure.

Other possible methods of identifying localized states are, for example, measuring the dc-conductance (see section 2.3.3) or testing the dependence on boundary conditions, as localized states should have exponentially small dependence on the boundary [Tho74]. However, those are more indirect methods which will not be used throughout this work.

5.1 Second Moment and Participation Number

Before introducing our new quantities, a short review on the commonly used methods might be helpful. The second moment or variance of a probability distribution is a well known quantity which is understood to give an estimate of the width of a probability distribution. Applied to the position representation of a quantum state, the variance provides a good measure for the spatial broadness of the state. For a discrete lattice with site index n and complex amplitude ψ_n the variance can be easily computed by:

$$(\Delta n)^2 = \left(\sum_{n=1}^{N} n^2 \cdot |\psi_n|^2 \right) - n_0^2$$

with $n_0 = \sum n \cdot |\psi_n|^2$ being the spatial center of the state.

Another concept to investigate the strength of localization is the Participation Number P introduced by Bell and Dean and defined via its inverse by:

$$P^{-1} = \sum_{n=0}^{N} |\psi_n|^4.$$

On a discrete lattice, the Participation Number roughly counts the number of lattice sites where the wavefunction is significantly larger than zero. So, if the wavefunction spreads over only L lattice sites with equal amplitude $|\psi_n|^2 = 1/L$ and vanishes elsewhere, we get a participation number of $P = L$.

For an exponentially decaying wavefunction $|\psi_n|^2 = A\exp(-|n-n_0|/\xi)$ with localization length ξ, as usually obtained in linear random lattices due to Anderson's results, we obtain the following: First of all, the normalization factor A is calculated as

$$A^{-1} = 2\sum_{n=0}^{\infty}\left(\mathrm{e}^{-1/\xi}\right)^n - 1 = \frac{2}{1-\mathrm{e}^{-1/\xi}} - 1 = \frac{\mathrm{e}^{1/\xi}+1}{\mathrm{e}^{1/\xi}-1} \approx 2\xi$$

The last approximation is valid for $\xi \gg 1$, which we assume from now on. Now the formula for the Participation Number gives

$$\begin{aligned} P^{-1} &= \sum_{n=-\infty}^{\infty}|\psi_n|^4 = A^2\left(2\sum_{n=0}^{\infty}\left(\mathrm{e}^{-2/\xi}\right)^n - 1\right) \\ &= A^2\left(\frac{2}{1-\mathrm{e}^{-2/\xi}} - 1\right) \\ &= A^2\left(\frac{\mathrm{e}^{2/\xi}+1}{\mathrm{e}^{2/\xi}-1}\right) \approx \frac{1}{4\xi} \end{aligned} \tag{5.1}$$

Thus, we get $P \approx 4\xi$ for this kind of distribution.

For an extended plane wave $\psi_n = e^{-ikn}/\sqrt{N}$ with wave number k, the participation number increases with N and diverges in the limit $N \to \infty$. So in a localized state, P gives an estimate for the degree of localization.

It is very reasonable to assume a correspondence between the Participation Number P and the second moment $(\Delta n)^2$. For the case of a continuous Gauss–distribution with variance $(\Delta x)^2$:

$$p(x) = \frac{1}{\Delta n\sqrt{2\pi}}\mathrm{e}^{-\frac{(x-x_0)^2}{2(\Delta x)^2}}, \tag{5.2}$$

a short computation for the Participation Number reveals

$$P^{-1} = \int_{-\infty}^{\infty}p^2(x)\mathrm{d}x = \frac{1}{(\Delta x)^2 2\pi}\sqrt{\pi(\Delta x)^2} = (2\Delta x\sqrt{\pi})^{-1} \tag{5.3}$$

and hence

$$P \sim \Delta x. \tag{5.4}$$

In this calculation a continuous probability distribution was used for the sake of simplicity. For $\Delta x \gg 1$ the infinite sums that would come up for discrete probability distributions are well approximated by the integrals above which justifies this approach.

The relation $P \sim \Delta x$ that was shown here to hold for Gauss-distributions must, of course, not be true for other kinds of distributions. For example, think of two peaks which move away from each other but have constant sizes. The Participation Number would remain constant in this case, but the second moment grows with increasing distance of the peaks. So one should always analyze both, second moment *and* Participation Number, to get a full picture of the spreading behavior.

5.2 Rényi Entropies and Generalized Participation Numbers

We have seen that the Participation Number is a good measure of spatial spreading when dealing with exponentially localized states. But from older results, we expect that nonlinearity in a random lattice destroys the exponentially localized states on a logarithmic timescale, leading to wavefunctions with a plateau around their center and exponentially decaying tails. The problem is that the whole distribution is disturbed by some very large noise due to the random character of the potential and the nonlinearity. Hence, the plateau usually consists of a complex peak structure which fluctuates rapidly on short time scales, while the width of the plateau is quasi constant on short times and varies only on a logarithmic time scale (subdiffusive $\sim t^{0.2}$). As the Participation Number mainly counts the number of peaks of the plateau, it also fluctuates very strongly on short time scales. Furthermore, there might be changes in the peak structure of the wavefunction during the spreading. Currently, it is assumed that the time average of the fluctuation becomes independent of the averaging interval. That means, the peak structure on average does not change during the spreading. However, to our knowledge it has not yet been investigated if this assumption is correct. This question will be numerically addressed later, but now some of the tools used there are introduced.

Our new approach is based on the idea of Rényi entropies and it generalizes the Participation Number by defining a new quantity P_q as follows:

$$P_q := \left(\sum_n |\psi_n|^{2q} \right)^{\frac{1}{1-q}}, \quad q \neq 1. \tag{5.5}$$

It is easy to see that the case $q = 2$ corresponds to the normal Participation Number $P_2 = P$. An interesting property of P_q is that for uniformly spread distributions where $|\psi_n|^2 = 1/L$ for precisely L lattice sites, P_q is independent of q: $P_q = P = L$. This is the reason for exponent $1/(1-q)$ in eqn. (5.5). Before discussing the meaning of the parameter q and the actual application of P_q, we quickly want to stress the relation between P_q and the general Rényi Entropies, which we denote I_q and defined by [Rén61]:

$$I_q := \frac{1}{1-q} \ln \sum_n |\psi_n|^{2q}. \tag{5.6}$$

Now it is easy to verify from (5.6) that the following important relation holds between the Participation Numbers and these entropies:

$$P_q = \mathrm{e}^{I_q}. \tag{5.7}$$

Using this result and the fact that in the limit $q \to 1$ the Rényi Entropy gives the usual entropy S

$$I_1 := \lim_{q \to 1} I_q = \sum_n |\psi_n|^2 \log |\psi_n|^2 =: S, \tag{5.8}$$

it is very reasonable to also define

$$P_1 := \mathrm{e}^S. \tag{5.9}$$

From eqn. (5.7) we have a one-to-one correspondence between Participation Numbers and Rényi entropies, which means they are equivalent and we can apply any properties for the Rényi entropies also to the generalized Participation Numbers.

5.2.1 Monotonic Behavior

Rényi entropies I_q are well known to mathematicians and their properties are widely explored [Rén61]. We only want to emphasize the monotonic dependence on the parameter q as is given by the following inequality:

$$I_q \leq I_r \qquad \text{for} \quad q > r \tag{5.10}$$

That means I_q is a *nonincreasing* function with q. For finite N, I_q is a sum of N differentiable terms in q and thus is differentiable itself yielding the following relation [BS93]:

$$\frac{\partial I_q}{\partial q} \leq 0. \tag{5.11}$$

As we specifically need the nonincreasing property for $q = 2$ and $r = 1$, we want to show it for these values explicitely. We start at *Jensen's inequality* with $(-\ln)$ as a convex function.

$$\begin{aligned} \frac{-\ln \sum p_i \cdot p_i}{\sum p_i} &\leq \frac{\sum p_i(-\ln p_i)}{\sum p_i} \\ -\ln \sum p_i^2 &\leq -\sum p_i \ln p_i \\ I_2 &\leq I_1 \end{aligned}$$

Note that from (5.7), we obviously also have

$$P_q \leq P_r \qquad \text{for} \quad q > r \tag{5.12}$$

5.2.2 Correlation of Rényi entropies

In particular, the monotonic behavior of I_q means that given the Shannon entropy $S[Q] = I_1[Q]$ of some probability distribution $Q = \{p_i, \quad i = 0 \ldots N\}$, we have a natural upper bound for $I_2[Q]$. Now, we also want to find a lower bound for $I_2[Q]$ for a given value of $I_1[Q]$. The existence of such a bound seems reasonable as one does not expect to find, for example, values of $I_2 \approx 0$ while $I_1 \approx \ln N$. It is natural to assume a correlation of the entropies for different q for a given fixed probability distribution Q. This assumption can be mathematically fortified and we will shortly restate the essential arguments provided in [Ż03]. Therefore, we introduce a special class of probability distributions Q_k which describe the occurrence of precisely k events of equal probability.

$$Q_k := \{p_n = 1/k \quad \text{for} \quad n \leq k, \quad p_n = 0 \quad \text{otherwise } \}. \tag{5.13}$$

For these distributions we can easily verify that $I_q[Q_k] = \ln k$, independent of q. From the Q_k we now construct interpolating probability distributions $Q_{k,l}(a)$ in the following way:

$$Q_{k,l}(a) := aQ_k + (1-a)Q_l \qquad 0 \leq a \leq 1. \tag{5.14}$$

Now Harremoës and Topsøe proved the following relation for any probability distribution Q with a known value $I_2[Q]$ [HT01]:

$$I_1[Q] \leq I_1[Q_{1,N}(a)], \tag{5.15}$$

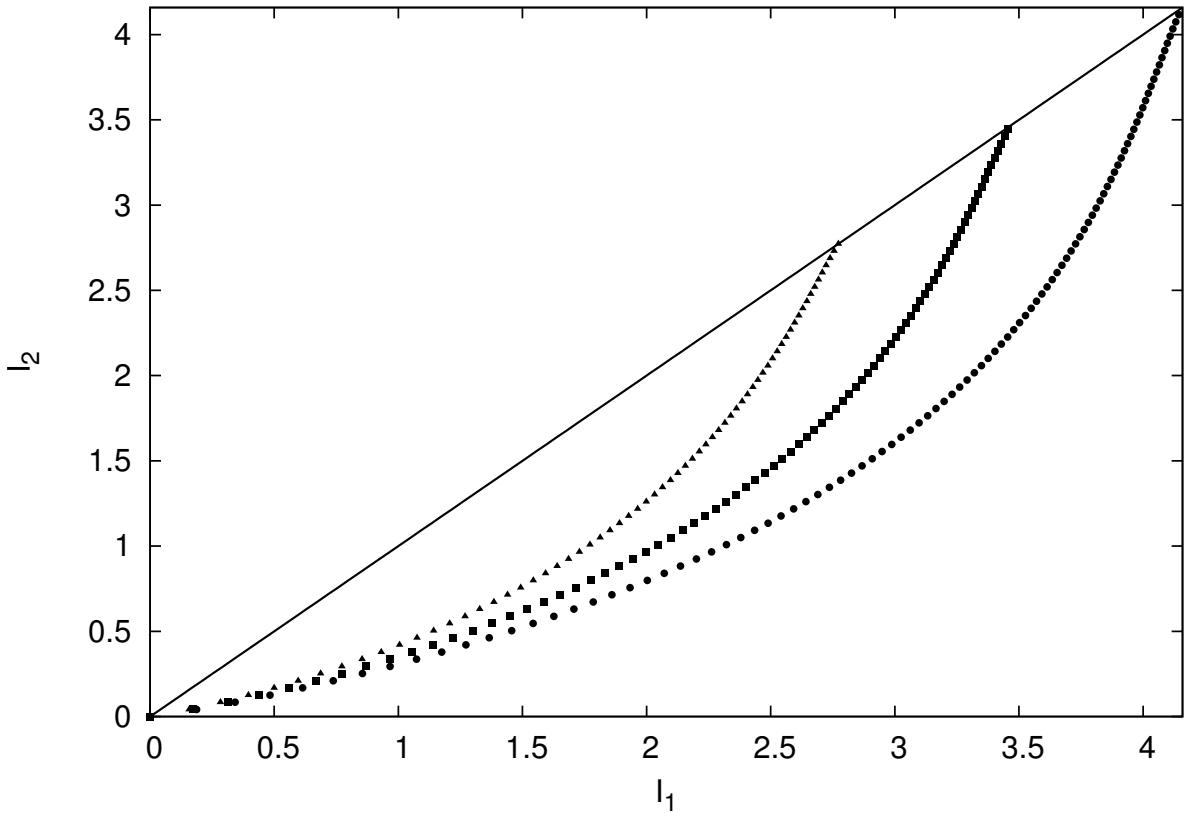

Figure 5.1: Bounds of the Rényi Entropy I_2 for given Shannon entropy $S = I_1$ and different system sizes $N = 16$ (triangles), $N = 32$ (squares) and $N = 64$ (circles). The straight line marks the upper bound for I_2, simply given by I_1. The points represent lower bounds depending on the size of the distribution N as (implicitly) given in (5.17) and (5.16). So given any distribution Q, we know that the value I_2 lies between the straight and the dotted line (depending on N) for a given I_1.

where a is determined by the given value of $I_2[Q]$ by the following condition:

$$I_2[Q] \stackrel{!}{=} I_2[Q_{1,N}(a)].$$

To prove (5.15), one has to show that for any given value of I_2 the corresponding interpolated distribution $Q_{1,n}(a)$ leads to the maximal possible value of I_1. This can be done by searching the boundary of the region of possible values in the I_1-I_2–plane at which the difference between I_1 and I_2 happens to be extremal. The complete reasoning can be found in [HT01], together with other relations between the entropies.[1]

We will use this result to obtain a lower bound for I_2 given $I_1 = S$. Let us compute $I_2[Q_{1,N}(a)]$, which simply gives

$$I_2[Q_{1,N}(a)] = -\ln\left(\frac{(1+(N-1)\cdot a)^2}{N^2} + (N-1)\frac{(1-a)^2}{N^2}\right).$$

[1] In [HT01] also a lower bound for $I_1[Q]$ is calculated from the boundary of the region, but we just use $I_2[Q]$ as it is sufficient and easier to understand.

Solving this for a yields

$$a = \sqrt{\frac{N \exp(-S_2) - 1}{N - 1}}, \tag{5.16}$$

while equation (5.15) leads to:

$$I_1[Q_{1,N}(a)] \leq (1 - N)\frac{1 - a}{N} \ln \frac{1 - a}{N} - \frac{1 + a(N - 1)}{N} \ln \frac{1 + a(N - 1)}{N}. \tag{5.17}$$

At this point, we should substitute a and solve for I_2 to get an analytic result for the lower bound of I_2 depending on I_1. But the result can not be written in closed form and we restrict ourselves to present it graphically in Fig. 5.1. As expected, the maximal possible difference between I_1 and I_2 vanishes for $I_1 \to 0$ and $I_1 \to N$ while for intermediate values of $I_1 \approx \ln(N/2)$ the possible difference between the entropies is maximal. Note that the difference of these values $I_1 - I_2$ is the structural entropy as defined in the next chapter, which is thus also bounded by this result.

5.3 Structural Entropy

As is well known, the usual Shannon entropy S can be interpreted as measuring the deviation of a distribution (p_i) from the uniform distribution $p_i = 1/N$. Now in our case, this deviation has two different origins: The first reason is the spatial localization of the wavefunction and the second reason is the complex peak structure due to the disorder and nonlinearity. We will try to separate these effects and find proper methods of measuring both individually. We apply some of the results developed in [PV92]. The idea is to consider the "proto-type" of a localized state as the steplike function where $p_i = 1/P$ on precisely P sites, and $p_i = 0$ everywhere else – the Participation Number for this state is then also P. This distribution has no peak structure at all and its entropy is simply given by $S = \ln P$. We use this to define the *localization entropy* S_{loc} that comes from the localized shape of the distribution:

$$S_{\text{loc}} = \ln P = I_2. \tag{5.18}$$

The second equality simply comes from (5.7). Now the complex peak structure and the exponential tails of the actual distribution are considered as a deviation from this steplike localized distribution and we write the entropy S as a sum of the localization entropy defined above and a term induced by the peak structure called *structural entropy* S_{str}

$$S = S_{\text{loc}} + S_{\text{str}}. \tag{5.19}$$

We solve that for S_{str} and write the result in terms of Rényi entropies and Participation Numbers:

$$S_{\text{str}} = I_1 - I_2 = \ln(P_1/P_2) \tag{5.20}$$

Note that from (5.10) follows that $S_{\text{str}} > 0$. Moreover, the results of section 5.2.2 also give an upper bound for S_{str} depending on S.

Thus, we have found a quantity that measures the influence of the peak structure by taking the deviation of the actual entropy from the entropy corresponding to an unstructured, localized, steplike distribution. So if the complexity of the peak structure and the localization shape does not change while the wavefunction spreads, we would observe a constant structural entropy S_{str}.

6 Structural Entropy of Delocalized States

In this chapter, the behavior of the structural entropy for different types of probability distributions is investigated. At first two analytic considerations are presented and in the third section some numerical results for randomly excited short lattices are shown. Eventually, spreading states in nonlinear disordered lattices are investigated.

6.1 Gauss–Distribution

The first distribution in question is the well known Gauss–curve:

$$|\psi(x)|^2 = \frac{1}{\Delta x\sqrt{2\pi}} \mathrm{e}^{-\frac{(x-x_0)^2}{2(\Delta x)^2}}. \tag{6.1}$$

A continuous spatial variable x is used instead of lattice index n for the sake of simpler calculations. From section 5.1 we know that the Participation Number of a Gauss-distribution is (5.3)

$$P = 2\Delta x\sqrt{\pi}, \tag{6.2}$$

while the entropy S can be calculated as

$$\begin{aligned} S &= -\int_{-\infty}^{\infty} |\psi|^2(x) \ln |\psi|^2(x) \mathrm{d}x \\ &= \frac{1}{\Delta x\sqrt{2\pi}} \int_{-\infty}^{\infty} \left(\frac{(x-x_0)^2}{2(\Delta x)^2} - \ln(\sqrt{2\pi}\Delta x) \right) \mathrm{e}^{-\frac{(x-x_0)^2}{2(\Delta x)^2}} \mathrm{d}x \\ &= \frac{\ln(\sqrt{2\pi}\Delta x)}{\sqrt{2\pi}\Delta x} \sqrt{2\pi(\Delta x)^2} + \frac{1}{2(\Delta x)^2}(\Delta x)^2 \\ &= \ln(\sqrt{2\pi}\Delta x) + \frac{1}{2}. \end{aligned}$$

Using this and eqn. (6.2), we find the structural entropy to be

$$S_{\mathrm{str}} = I_1 - I_2 = S - \ln P = \frac{1}{2} - \frac{1}{2}\ln 2 \approx 0.153, \tag{6.3}$$

which is independent of Δx. So for a widening Gauss-packet, the structural entropy remains constant.

6.2 Exponentially Decaying States

Now the structural entropy for exponentially decaying distributions is calculated. The shape of the state is as follows:

$$|\psi_n|^2 = A\mathrm{e}^{-|n|/\xi}, \qquad A \approx \frac{1}{2\xi}.$$

We again use the results from section 5.1 where the Participation Number was obtained (5.1):

$$P \approx 4\xi.$$

The entropy of such a state can be computed as

$$\begin{aligned} S &= \sum_{n=-\infty}^{\infty} |\psi_n|^2 \ln |\psi_n|^2 = -\ln A + \frac{2A}{\xi} \sum_{n=0}^{\infty} n \mathrm{e}^{-n/\xi} \\ &= -\ln A + \frac{2A}{\xi} \frac{\mathrm{e}^{-1/\xi}}{(1-\mathrm{e}^{-1/\xi})^2} \\ &\approx \ln(2\xi) + 1 - \frac{1}{\xi}. \end{aligned} \tag{6.4}$$

which gives the following result for the structural entropy:

$$S_{\mathrm{str}} = S - \ln P \approx 1 - \ln 2 - \frac{1}{\xi} \approx 0.3 - \frac{1}{\xi}. \tag{6.5}$$

Here we find a small dependence on the localization length, but this vanishes for large ξ, where S_{str} converges to approximately 0.3.

6.3 Random States in Short Lattices

In this section, the structural entropy of random distributions is investigated. The random distributions are created by the time evolution of a state in a random nonlinear lattice – the DANSE model. More precisely, we initialize the wavefunction in a short lattice with random values between 0 and 1: $|\psi_n|^2 = \mathrm{rand}(0,1)$ Then the time evolution according to the DANSE is started and we compute S_{str} after waiting some time $t = 10^4$. The parameters were set to $W = 4$, $\beta = 1$ and $\alpha = 1$ and the lattice size was chosen from $N = 7 \ldots 100$. The idea is to find out if and how the structural entropy of typical, extended wavefunctions with complex peak structure depends on the width of the wavefunction. The width is controlled by the different sizes N and the choice of random initial conditions ensures that the whole lattice is excited. To avoid fluctuations, the entropies were averaged over a time window of $t = 10^4$.

The numerical results can be seen in Figure 6.1. The entropy S and the Participation Number P, the localization entropy $S_{\mathrm{loc}} = \ln P$ respectively, exhibit the expected behavior: logarithmic growth with system size. The more interesting quantity is the structural entropy S_{str} that turns out to remain constant for different lattice sizes, at least for $N > 20$. The important conclusion is that the peak structure of wavefunctions induced by time evolutions according to the DANSE model is independent of the extension of the wavefunction. This behavior is, however, not unexpected, but the result is still important for the interpretation of spread wavefunctions in large lattices. The value found for S_{str} is approximately 0.25 for these random distributions. Now the structural properties of subdiffusively spreading wavefunctions in long random nonlinear lattices can be investigated and compared to the above findings. This will be done in section 7.4.

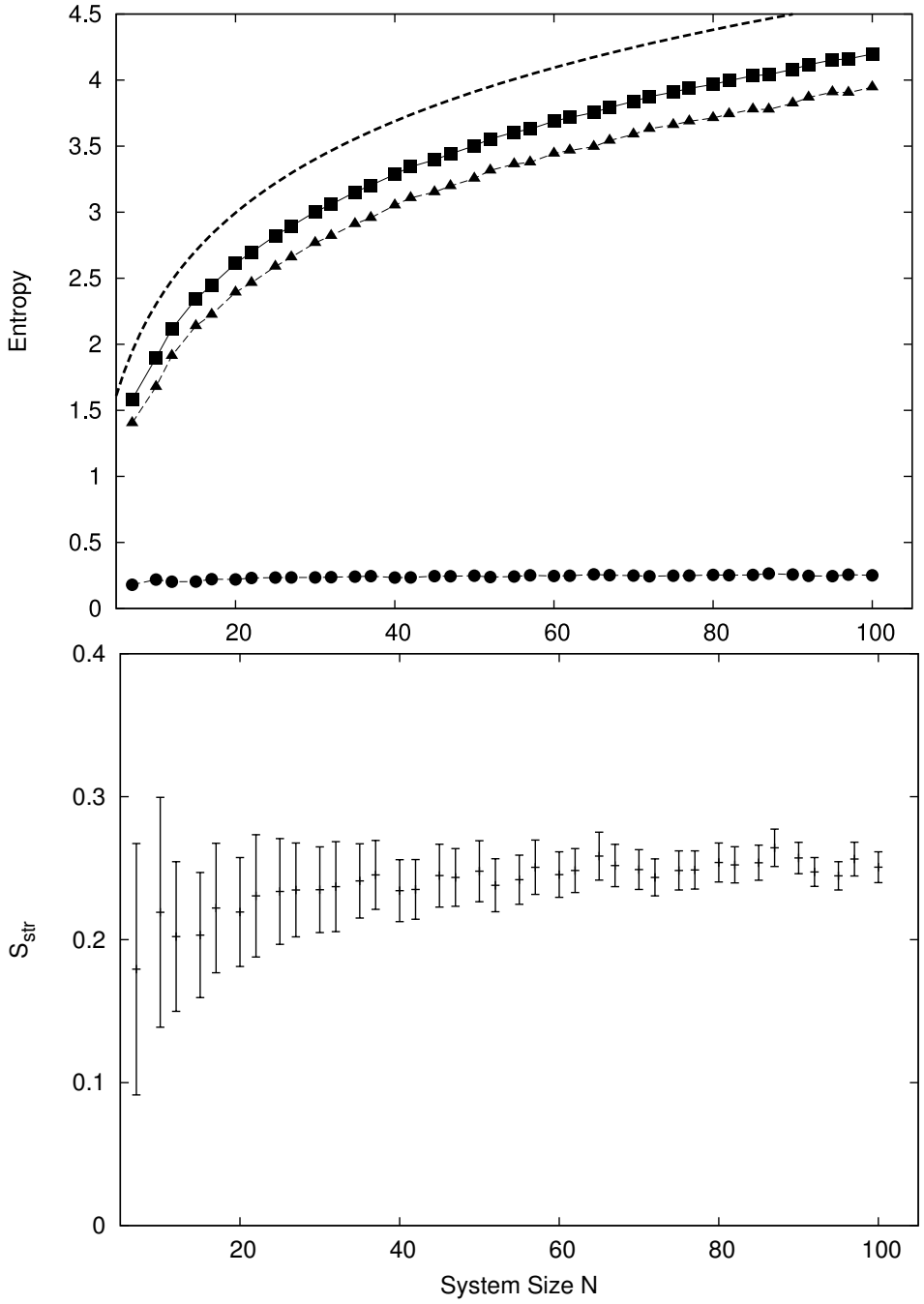

Figure 6.1: Entropies for a completely excited lattice vs lattice size N. Disorder strengths of the random potential was always $W = 4.0$. The entropies are time averages of randomly distributed initial conditions where the average was taken from $t = 10^4$ until $t = 2 \cdot 10^4$, nonlinear strength was set to $\beta = 1.0$. The top plot shows entropies $S = I_1$ (squares), I_2 (triangles) and the structural entropy $S_{\mathrm{str}} = I_1 - I_2$ (points) for different lattice sizes N between 7 and 100. While the entropies S and I_2 increase logarithmically with lattice size (black dashed line is the curve $\ln N$), the structural entropy is independent of the system size. Bottom graph shows S_{str} with errorbars coming from the averaging over disorder realizations. It clearly shows that for $N > 20$, the structural entropy is nearly constant $S_{\mathrm{str}} \approx 0.25$ except for some fluctuations.

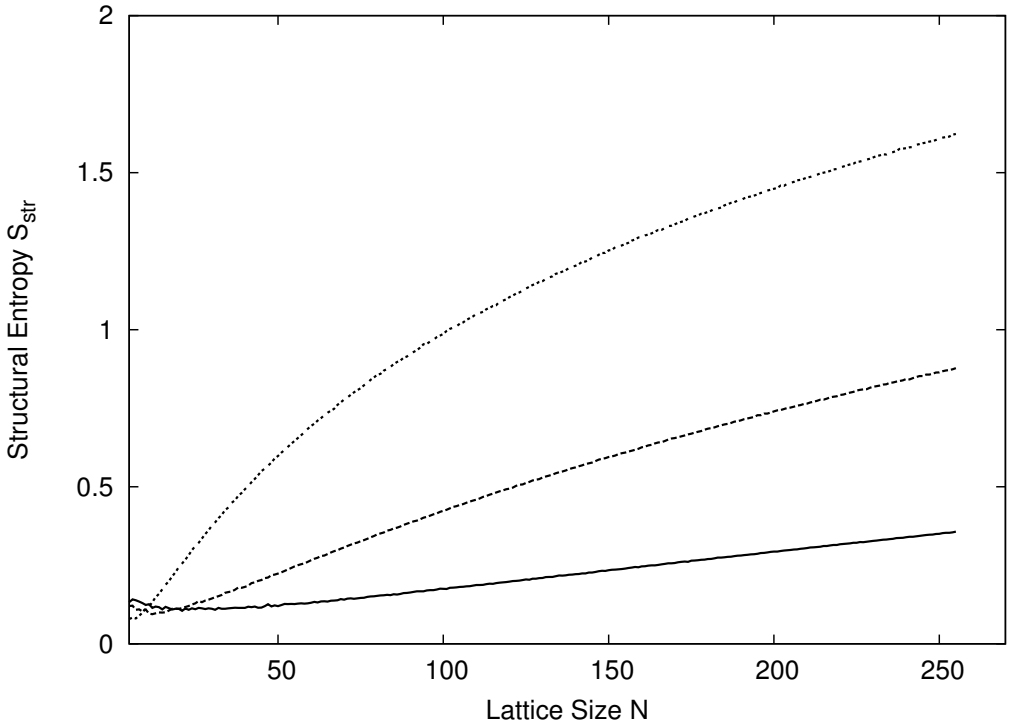

Figure 6.2: Structural Entropy for distributions with remaining peaks. The curves correspond to different fractions of the background noise f (see text). Top curve is $f = 0.8$, middle curve is $f = 0.9$ and the bottom curve is $f = 0.95$. So even if 95% of the distribution spread and only 5% remain localized at some lattice site, a clear increase of the structural entropy is observed.

6.4 Remaining Peaks in Short Lattices

The last setup that will be investigated before considering the actual gDANSE system is a spread background noise with random peak structure superposed by a single peak at one lattice site. This constructions resembles the case when some part of the wavefunction spreads across the lattice while the other part remains localized at some site(s). This partial localization might be caused by partially excited breathers, as suggested by Kopidakis et al. [KKFA08], for example. We now want to study how the structural entropy behaves in this case. Therefore, a finite lattice of size N is initialized with an uniform random distribution across $N-1$ sites. This part of the distribution is normalized to $f < 1$. The probability value of the remaining lattice site is then set to the value $1 - f$ which ensures that the total norm over all sites is equal to 1. Finally, the structural entropy of such a state is calculated and averaged over many realizations of the random part of the distribution. The spreading of the random part can then be modeled by increasing the lattice size N while keeping the fraction of random background f constant. This was done for several values $f = 0.8, 0.9, 0.95$ and the results are presented in Fig. 6.2.

The main point is that the structural entropy shows a clear increase for all values of f. Especially, even if 95% of the initially localized probability spreads across the lattice and only 5% remains localized, we can still observe a clear increase of the structural entropy and hence identify such behavior by analyzing S_{str} during the spreading.

7 Spreading Behavior

In this chapter, one of the major results of this work will be presented. The spreading behavior of the gDANSE system (see section 4.1) with various nonlinear indices $\alpha = 0.5, 1, 2, 3$ is studied analytically and numerically. First of all, a theoretical analysis of the spreading law is presented. The spreading exponents obtained from those calculations are then compared with numerical results for the spreading in the gDANSE model. For a brief description of the general mechanisms of spreading in nonlinear disordered lattices see section 4.3.2.

7.1 Theoretical Derivation of the Spreading Exponents

The main purpose of this work is the investigation of the spreading behavior of initially localized states in a system with disorder and nonlinearity. The first results on this topic were obtained by D. L. Shepelyansky in 1993 [She93], who found subdiffusive spreading of initial delta peaks for a large enough nonlinearity $\beta > \beta_{\text{crit}}$. In his article, also an approximation for the spreading law was given. In the following, a calculation of the spreading law based on the diffusion equation is presented.

The spreading is induced by the nonlinear mode interactions and it can be described by a nonlinear diffusion equation for the probability density $\rho = |\psi|^2$:

$$\frac{\partial \rho}{\partial t} = \frac{\partial}{\partial x}\left(\rho^a \frac{\partial \rho}{\partial x}\right). \tag{7.1}$$

The diffusion coefficient is already replaced by a power law dependence $D \sim \rho^a$ with an unknown exponent a which should depend on the nonlinear index α. This diffusion equation has a self similar solution [Tuc76]:

$$\rho(x,t) = \begin{cases} t^{-1/(2+a)} f(x/t^{1/(2+a)}) & \text{for} \quad x < x_0 \\ 0 & \text{for} \quad x > x_0 \end{cases} \tag{7.2}$$

with

$$f(y) = \left(B - \frac{a y^2}{2(a+2)}\right)^{1/a}, \tag{7.3}$$

where B is some integration constant. x_0 is the front of the diffusion and has the following time dependence:

$$x_0 = \sqrt{2B\frac{2+a}{a} t^{2/(2+a)}} \sim t^{1/(2+a)}. \tag{7.4}$$

Going back to spatially discretized wavefunctions, this means that the number of sites where $|\psi_n|^2$ is nonzero also grows as $\sim t^{1/(2+a)}$, and hence we find for the Participation Number and the second moment:

$$P \sim t^{1/(2+a)}, \qquad (\Delta n)^2 \sim t^{2/(2+a)}. \tag{7.5}$$

The question on the relation of a and α is still open. To our understanding, there are three possibilities:

"strong stochasticity": $a = 2\alpha$. This is equivalent to the results presented in appendix B.1 and leads to the spreading exponent:

$$\gamma_A = 1/(1+\alpha). \tag{7.6}$$

"weak stochasticity": $a = 3\alpha$. This leads to a spreading with the exponent:

$$\gamma_B = 2/(2+3\alpha), \tag{7.7}$$

which is the same as the first results from Shepelyansky in [She93].

"very weak stochasticity": $a = 4\alpha$ gives the spreading exponent as

$$\gamma_C = 1/(1+2\alpha), \tag{7.8}$$

and is equivalent to the results from Flach et al. [FKS09] which are shown in appendix B.2.

Older numerical results seem to support the "weak" or "very weak" stochasticity assumption by showing a spreading exponent of $\gamma \approx 0.35$ for $\alpha = 1$ [PS08, She93]. However, until now this has not been checked for other values of α and we try to investigate that in the next sections.

7.2 Numerical Setup

We used a large lattice of size $N = 1024$ with a random potential with disorder strength $W = 4.0$. The nonlinear strength β was set to 1 for all simulations. Note that these parameter values lie within the region where spreading should be present (compare section 4.3.2). The system was initialized with a single peak at one lattice site and the energy of this state was ensured to lie close to the band center $-1 < E < 1$. Then a time evolution according to the gDANSE (4.2) was applied with different nonlinear indices $\alpha = 0.5, 1, 2, 3$. For the numerical time evolution we used the Crank-Nicolson scheme (see section 4.4) with a step size $\Delta t = 0.1$ and we ran simulations up to 10^9 timesteps, which means a total time of $t = 10^8$. One of these runs took about six days on a 3 GHz processor. This procedure was repeated for 16 different disorder realizations for each α, which means a total of 64 runs. During the time evolution, the Participation Number and the second moment of the states were computed at logarithmic time intervals and averaged over small time windows. We chose the intervals logarithmically to have equidistant spacing of measurement points on a logarithmic timescale.

7.3 Spreading Exponents

To analyze the spreading behavior of the wavefunctions we fitted the data points for P and $(\Delta n)^2$ for each disorder realization separately and then computed the average and standard deviation for this set of exponents. The results are presented in Table 7.1 together with the

α	0.5	1	2	3
γ from fit $(\Delta n)^2 \sim t^\gamma$	0.56 ± 0.04	0.31 ± 0.04	0.18 ± 0.04	0.14 ± 0.05
γ from fit $P \sim t^{\gamma/2}$	0.53 ± 0.05	0.33 ± 0.05	0.21 ± 0.06	0.18 ± 0.06
γ_A (strong stochasticity)	0.67	0.50	0.33	0.25
γ_B (weak stochasticity)	0.56	0.40	0.25	0.18
γ_C (very weak stochasticity)	0.50	0.33	0.20	0.14

Table 7.1: Comparison of numerical results and theoretical expectation from equations (7.6), (7.7) and (7.8) for the exponent in the power law spreading $(\Delta n)^2 \sim t^\gamma$. For all values α, the theoretical values γ_C seem to give the best description of the spreading, but γ_B is also close. The assumption of strong stochasticity, however, gives spreading exponent which are definitely higher than the numerical observations.

theoretical values from section 7.1. A graphical presentation of the results is given in Fig. 7.1 that shows averages over the disorder realizations of P and $(\Delta n)^2$ (points) and the fitted growth (lines) for all investigated values of α.

First of all, our simulation verifies former results for $\alpha = 1$ and seems to support the assumptions of weak and/or very weak stochasticity. For $\alpha = 1$, a spreading exponent of $\gamma \approx 0.32 \pm 0.04$ was found which is in good agreement with the prediction $\gamma_C = 0.33$. The value $\gamma_A = 0.5$ obtained for "strong stochasticity" is clearly larger than our numerical results and we conclude that, following the arguments in appendix B.2, our simulation also supports the idea of some kind of downscaling of spreading. For $\alpha = 0.5$, the numerics show a slightly stronger spreading than given by the theory $\gamma_C = 0.5$, and lie closer to γ_B. For $\alpha = 2, 3$, we also have a good agreement of the numerical resulta with the theoretical values γ_C, γ_B. But as the spreading is very slow for these α, fluctuations play a stronger role leading to errors in measurement up to 30%.

To get a better idea of the spreading, we also plotted the wavefunctions at the end of the integration $t = 10^8$ in left panel of Fig. 7.2. The plotted curves represent averages of the wavefunctions over disorder realizations and small time windows. The stronger spreading for smaller α is very obvious in this plot. For $\alpha = 2$ and $\alpha = 3$ the width of the wavefunction is rather small, but still clearly broader than for the linear case ($\beta = 0$). For $\alpha = 0.5$, it seems that we have reached the edges of the lattice after $t = 10^8$ which means that the boundary conditions (periodic in this case) should come into play and the spreading should stop. But looking at the wavefunction for a single disorder realization, one still sees a gap with exponentially decreasing values down to 10^{-20}. Those gaps are at different positions for different disorder realizations and after averaging none of them remains. Anyhow, for the lattice size $N = 1024$ and $\alpha = 0.5$ the maximum spreading time is $t = 10^8$, after which an influence of the boundary conditions come into play.

In the right panel of Fig. 7.2, wavefunctions for different α at different times are shown. Again the curves are averages over disorders[1] and short time windows and they are shifted vertically for better visibility. The shapes of those wavefunctions are very similar and this fortifies the assumption that higher nonlinear indices only slow down the spreading but do not change the mechanisms.

[1] The disorder realizations were the same for different α.

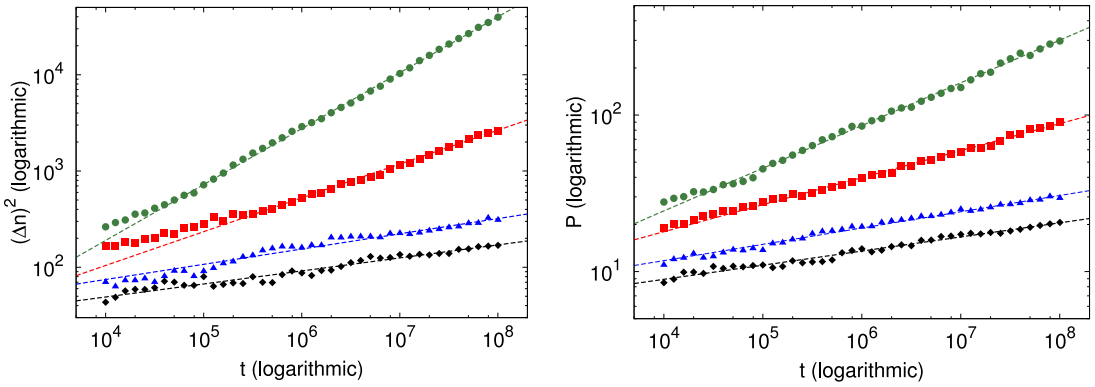

Figure 7.1: Time evolution of the second moment $(\Delta n)^2$ (left panel) and the Participation Number P (right panel) for different nonlinear exponents α. The values are averaged over 16 disorder realizations and small time windows. Different colors belong to different values of the nonlinear exponent α: green: $\alpha = 0.5$, red: $\alpha = 1$, blue: $\alpha = 2$, black: $\alpha = 3$. The plots show a clear increase of both $(\Delta n)^2$ and P in a subdiffusive way. Smaller α lead to stronger spreading, but even for $\alpha = 3$, the wavefunction was doubtlessly spreading in our simulation. The dashed lines are fits $\sim t^\gamma$ – see Table 7.1 for the fitted values.

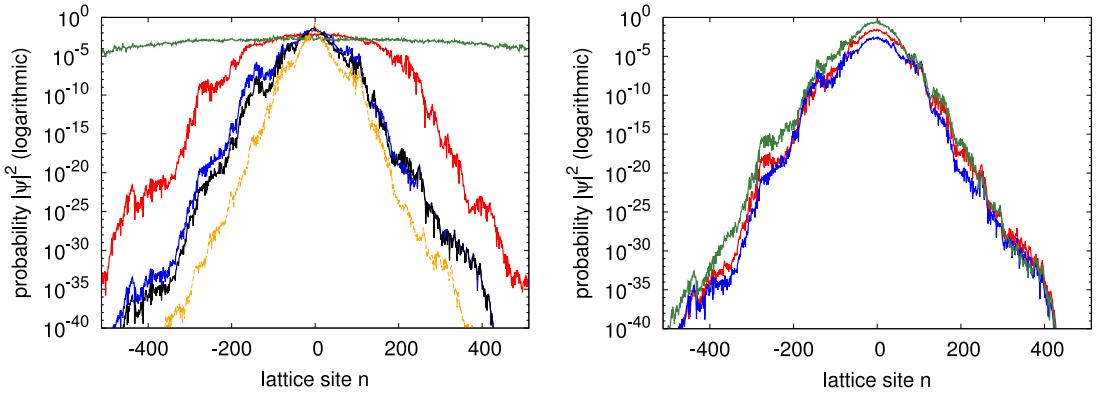

Figure 7.2: **Left:** Wavefunctions at time $t = 10^8$. Plotted are the probabilities $|\psi_n|^2$ at lattice sites n for initial delta peaks at lattice site $n_0 = 0$. Different colors indicate nonlinear exponents: green: $\alpha = 0.5$, red: $\alpha = 1$, blue: $\alpha = 2$, black: $\alpha = 3$ – for comparison the wavefunction for the linear case is also shown (orange $\beta = 0$). The wavefunctions were averaged over time windows and 16 disorder realizations. The red curve ($\alpha = 1$) exhibits a clear plateau from the spreading. For $\alpha = 0.5$, even the whole lattice was excited after $t = 10^8$ which means we should have chosen it larger. Fortunately, we don't see influences of the boundary in P or $(\Delta n)^2$ quite yet (see Fig. 7.1). The cases $\alpha = 2$ and $\alpha = 3$ are quite close together, but both are clearly more spread than for zero nonlinearity (orange). **Right:** Comparison of different times for different nonlinear exponents: green: $\alpha = 0.5$, $t = 10^4$ (shifted upwards), red: $\alpha = 1$, $t = 10^5$ (unshifted), blue: $\alpha = 2$, $t = 10^8$ (shifted downwards). They show very similar shape which indicates that different nonlinear indices only influence the spreading time, not the spreading mechanism.

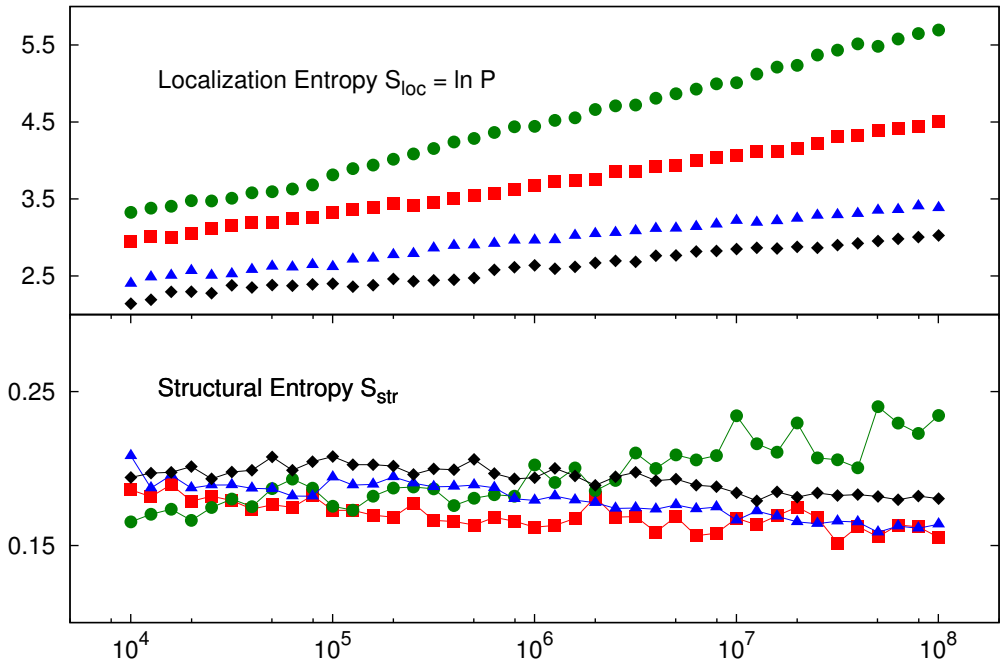

Figure 7.3: Time evolution of the localization entropy $S_{\rm loc}$ (top) and the structural entropy $S_{\rm str}$ (bottom) for different nonlinear strength α. x-axis is time t in logarithmic scaling. Color coding as in Fig. 7.1: green: $\alpha = 0.5$, red: $\alpha = 1$, blue: $\alpha = 2$, black: $\alpha = 3$. The top plot is essentially the same as the right panel in Fig. 7.1 as $S_{\rm str} = \ln P$. Values are averaged over time windows and 16 disorder realizations. The plot shows a small decrease of $S_{\rm str}$ for $\alpha \geq 1$ compared to the increase of $S_{\rm loc}$, while for $\alpha = 0.5$ the structural entropy also increases.

7.4 Structural Entropy of Spreading States

Now we want to apply our new tool $S_{\rm str}$ to the gDANSE model with initially localized states in large lattices. We used the same data as in the last section, but now the structural entropy $S_{\rm str}$ was analyzed for the different nonlinear indices α.

Again, for each value of α the time evolution was done for 16 different disorder realizations and the obtained values are averages over these realizations and usually also averaged over small time windows to surpress random fluctuations. For each such time evolution, the entropies of the states were computed at logarithmic time intervals.

The results are presented in Fig. 7.3. The localization entropy $S_{\rm loc} = \ln P$ is clearly increasing for all values of α, as seen before, but the structural entropy $S_{\rm str}$ remains rather constant. Although a small decreasing of $S_{\rm str}$ is visible for $\alpha \geq 1$, the strength of decrease is very small compared to the strength of the spreading. Numerical fits $S_{\rm str} \sim \nu \log t$ gives values $\nu \approx -0.002 \ldots -0.004$ for $\alpha \geq 1$, which is two orders of magnitude smaller than the spreading which is about $S_{\rm loc} \sim 0.1 \ldots 0.2 \log t$. However, an oddity for $\alpha = 0.5$ is observed as for this value, the structural entropy is clearly increasing in contrast to the other cases. But a fit of this curve also gives a factor of the same magnitude as the others $\nu \approx 0.006$ and thus much smaller than the spreading. Despite this, we conclude that the structural properties of spreading wavefunctions in the gDANSE model remain unchanged.

Potential	$(\Delta n)^2 \sim t^\gamma$		$P \sim t^{\gamma/2}$	
$W = 4$	CN	FFT	CN	FFT
0	0.33	0.31	0.32	0.37
1	0.27	0.27	0.33	0.32
2	0.36	0.32	0.31	0.30
3	0.38	0.40	0.43	0.44
4	0.32	0.28	0.32	0.28
5	0.33	0.30	0.28	0.28
6	0.44	0.41	0.28	0.28
7	0.39	0.39	0.40	0.43
mean	0.35	0.33	0.34	0.34

Table 7.2: Measured exponents of the time evolution of $(\Delta n)^2$ and P for different integration schemes: Crank-Nicolson (CN) and Fast Fourier Transform (FFT). Both integration schemes give very similar results.

7.5 Results from FFT Integration

When using numerical simulations, there is always a chance that some observed effects might be numerical artefacts instead of physically relevant results. We tried to overcome this problem by applying a different integration scheme (Fast Fourier Transform) and comparing the spreading with the former results obtained by Crank-Nicolson integration. See section 4.4 for details on the different integration methods.

Both integrators were started with the same potential realization and the same initially excited lattice site. We investigated only the case $\alpha = 1$ here. The second moment and the Participation Number were measured in the same way and we fitted the growth rate $\sim t^\gamma$ separately for each disorder realization. Table 7.5 shows the obtained exponents for each realization and the mean value. The values do deviate for some realizations, but on average both integration methods gave similar results for the spreading exponent. Some simulations for smaller $\Delta t = 0.01$ exhibited the same behavior and we are confident that the observed spreading is not a numerical effect. This is also fortified by the results from other groups on this topic where different integration schemes were applied [PS08, She93] and similar results were obtained.

Part III

Thermalization in Short Lattices

In this part, the dependence of the spreading behavior of localized states on their energy will be investigated. In section 2.3.2, it was pointed out that the localization length of an eigenmode of the (linear) Anderson model depends on the eigenenergy of this state. In terms of eigenmodes, the spreading is induced by the nonlinear coupling. Furthermore, the coupling strength depends on the spatial overlap of the modes and hence is related to the localization length of these modes. In the former chapters, the initial conditions were chosen such that their energy is close to the band center. The corresponding eigenmodes most likely have comparably large localization length which supports the spreading.
So in our next study, many localized initial conditions with energies throughout the whole spectrum are chosen and their spreading behavior is investigated. In contrast to the former simulations, numerics are done for short lattices of $N = 16 \dots 64$ and the nonlinear index is set to 1 (normal DANSE) throughout this part. The main reason is to keep simulation time small as many runs for different energies are necessary. Additionally, we only distinguish between spreading and non-spreading states without addressing the spreading exponent. Spreading, non-spreading respectively, is identified roughly by the fraction of excited sites after a specific time – if the state was spreading, almost the whole lattice should be excited, otherwise only a small part of it. We will be using the term *thermalization* in this regard, which is introduced in the next chapter. Note, however, that the formal analogies to thermodynamics are not necessarily of physical relevance.

8 Thermalization

Originally, the term "thermalization" is used to describe the tendency of a system to establish a state in *thermal equilibrium*. In thermal equilibrium, energy is shared equally in its various forms. To reach this from arbitrary initial conditions, energy exchange between all of the energy-forms must be possible within the system. Usually, this is ensured if the system is *ergodic*. Ergodicity means that the probability of a typical trajectory to visit a certain phase space volume is proportional to the volume size. One might also say, that most[1] of the phase space points are visited with equal probability by typical trajectories.

8.1 Thermalization of Coupled Oscillators

These aspects will be applied to a disordered chain of coupled oscillators. Taking the eigenmode base, the various forms of energy are just the excited eigenmodes. From this, it immediately becomes clear that linearly coupled harmonic oscillators will not thermalize, because the amount of excitation of eigenmodes is constant in time and no energy transfer between them is possible. Adding nonlinear coupling of eigenmodes (using nonlinear oscillators), ergodicity might be created. Generally, it is very difficult to strictly show that a system is ergodic, but it is understood that the presence of chaos is a good hint to expect ergodicity as well, at least in some parts of the phase space. Chaos can be identified by calculating the largest *Lyapunov* exponent λ_1 of the system (e.g. [Ott93]). Fig. 8.1 shows the results of a numerical study on the Lyapunov exponent for short disordered lattices with the same parameters as chosen in the later chapters of this part, that is $N = 16, 32, 64$, $W = 4.0$, $\beta = 1.0$. The values are averaged over 12 disorder realizations and we found positive Lyapunov exponents $\lambda_1 > 0$ for all considered lattice sizes. Chaos in those chains is, however, rather weak and for larger lattice sizes, λ_1 even decreases further. Because chaos is so weak, it remains interesting to study thermalization itself. So whereas chains of linearly coupled harmonic oscillators do not thermalize, the nonlinear coupling might induce thermalization.

Note, that due to the energy conservation within the system, a thermalized state is generally not given by a uniform excitation of eigenmodes $|C_m|^2 \sim 1/N$. In fact, one finds Boltzmann-distributions by searching for states with maximal entropy for a given energy. This will be shown in the next section.

8.2 Maximum Entropy

How should thermalization be measured? To answer this, one first has to explain what thermalization means. In thermodynamics, a state is called to be in thermal equilibrium if

[1] Most means all except a subset of zero measure.

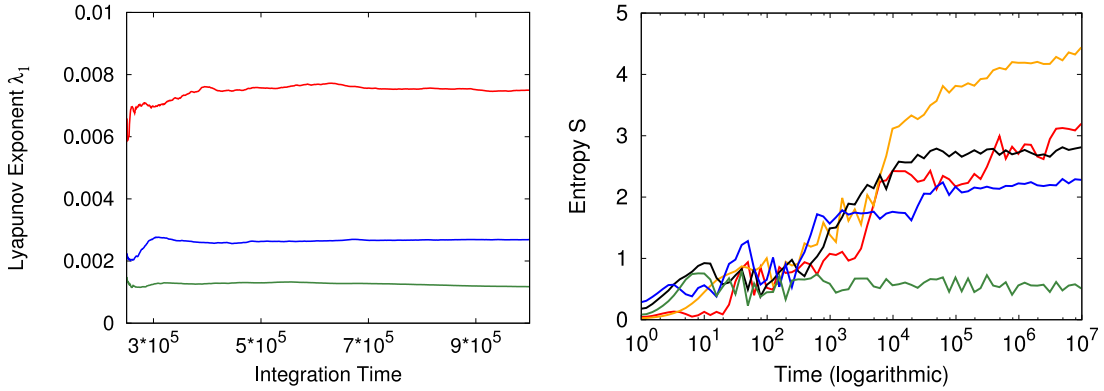

Figure 8.1: Left: Lyapunov exponents of disordered nonlinear lattices. Different colors mean different lattice sizes – top to bottom: $N = 16$ (red). $N = 32$ (blue) and $N = 64$ (green). The values are time averages starting from $t = 2.5 \cdot 10^5$ and also averaged over 12 disorder realizations. Parameters were $W = 4.0$ and $\beta = 1.0$. We see positive Lyapunov exponents for all three cases, but λ_1 decreases with lattice size. However, chaos, although weak, is present in these systems. **Right:** Time evolution of the entropy of initially localized states with different energies $E = 0.04$ (top, orange), $E = 2.01$ (second, red), $E = 2.15$ (third, black), $E = 2.49$ (fourth, blue), $E = 2.58$ (last, green – order at $t = 10^7$) for a large lattice of size $N = 1024$, $W = 4.0$, $\beta = 1.0$. States close to the band center seem to spread more than those at the band edges.

it has maximal entropy. This concept will be used here as well and so our tool to measure thermalization is the usual entropy:

$$S = \sum_m |C_m|^2 \ln |C_m|^2. \tag{8.1}$$

In chapter 5, different methods to measure localization were introduced and the Participation Number was presented as the first choice. Later, it was numerically observed that the difference $S_{str} = S - \ln P$ remains constant for spreading states in disordered nonlinear chains. We now stress this result and conclude that the entropy S is not only useful to measure thermalization, but also gives an idea on the spreading behavior.

The usage of S gives us the ability to apply well known results for states in thermal equilibrium – thermalized states. As said above, a system is known to have reached thermal equilibrium if its entropy is maximal. This can be mathematically formulated as a variational problem and we will shortly present the calculation for a linear chain of random oscillators. As we have two conserved quantities, the norm $\mathcal{N} = \sum |C_m|^2 = 1$ and the energy $E = \sum \epsilon_m |C_m|^2$, the equations of variation for the entropy read

$$\left(\frac{\partial S}{\partial |C_m|^2} + \lambda \frac{\partial \mathcal{N}}{\partial |C_m|^2} + \kappa \frac{\partial E}{\partial |C_m|^2} \right) \delta S = 0 \quad \forall m = 1 \dots N. \tag{8.2}$$

As δS is arbitrary, the term in brackets must be zero for each m separately. λ and κ are Langrange parameters of the variation. This is solved by the Gibbs distribution, which is sometimes also called Boltzmann distribution:

$$|C_m|^2 = \frac{1}{Z} \mathrm{e}^{-\kappa \epsilon_m}, \quad \text{with} \quad Z = \sum_m \mathrm{e}^{-\kappa \epsilon_m}. \tag{8.3}$$

Z is called *partition function* and ensures the normalization. This result has a formal analogy to a thermodynamic system with N microstates with energies ϵ_m connected to a heat bath and described by a canonical ensemble (see any textbook on statistical physics, e.g. [bac99]). The parameter κ would represent the (inverse) temperature of the heat bath in that case. However, this analogy is only formal and should not be considered as physically relevant. A real thermodynamic approach to a system of coupled oscillators in a heat bath would be mathematically more challenging.

The ϵ_m are the eigenenergies of the system and are randomly distributed within some interval $[-\Delta, \Delta]$, as shown in eq. (2.10), and with the mean value of approximately zero $\bar{\epsilon} \approx 0$. Note that ϵ_m can be negative in our system, hence the state energy E might also be negative which requires negative κ as well.

Given such a thermalized state, the entropy can be calculated as

$$S = \kappa E + \ln Z. \tag{8.4}$$

Keep in mind that κ, Z and E are not independent. Given κ, we can uniquely compute the energy E and Z, while for a given E the values for κ and Z are also determined.

The above result for a thermalized state (8.3) was calculated without the nonlinear term. If one wants find a solution for the whole system including nonlinearity, one has to use the complete expression for the energy where the nonlinear term appears. But for thermalized states that are spread over many eigenmodes, we find that the nonlinear energy is small and we neglect it in our discussion. This is not true at the edges of the energy band, where basicly only a few eigenmodes are effectively excited and the nonlinear energy might be large.

Now we have the following situation: given a specific disorder realization for the usual DANSE system, we can compute the eigenenergies by diagonalization and obtain the entropies of thermalized states for a given κ from the above calculations. From κ, we also can compute the energy of this state and obtain the curve $S(E)$ – entropy in dependence of energy for thermalized states – implicitely, by ranging κ from $-\infty$ to ∞. After adding nonlinearity, thermalized states close to the band center still follow the Boltzmann distribution because nonlinear corrections are small in this case.

8.3 Averaging

However, our goal is to find nonrandom properties that are independent of the disorder realization. To get those, an averaging over potential realizations has to be done. Let us first compute the averaged partition function $\langle Z \rangle$. Z is a function of N random variables $\epsilon_1, \epsilon_2, \ldots, \epsilon_N$. So the integration has to be done over those N variables:

$$\langle Z \rangle_\Omega = \left\langle \sum_{m=1}^{N} \mathrm{e}^{-\kappa\epsilon_m} \right\rangle_\Omega = \int_{-\infty}^{\infty} \cdots \int_{-\infty}^{\infty} p(\epsilon_1, \ldots, \epsilon_N) \sum_{m=1}^{N} \mathrm{e}^{-\kappa\epsilon_m} \mathrm{d}\epsilon_1 \ldots \mathrm{d}\epsilon_N. \tag{8.5}$$

$\langle \cdot \rangle_\Omega$ denotes the averaging over disorder realizations ω and $p(\epsilon_1, \ldots, \epsilon_N)$ is the probability of the set of random variables $\{\epsilon_1, \ldots, \epsilon_N\}$. To proceed further, we have to make two assumptions: Firstly, we assume that the ϵ_m are independent random variables. It follows that the

cumulative probability function can be written as a product

$$p(\epsilon_1, \ldots, \epsilon_N) = p(\epsilon_1) \cdot \ldots \cdot p(\epsilon_N) = \prod_m p(\epsilon_m). \tag{8.6}$$

Secondly, we assume $p(\epsilon_m) = \text{const} = 1/(2\Delta)$ if $-\Delta < \epsilon_m < \Delta$ and 0 otherwise, which means a constant density of states for the system. This assumption is supported by the results of section 2.3.2, but only valid for large disorders $W \gtrsim 4.0$ (see Fig. 2.1) and neglects the Lifshitz tails at the band edges. Using these assumptions, we can calculate the integrals and get:

$$\begin{aligned}
\langle Z \rangle_\Omega &= \frac{1}{(2\Delta)^N} \int_{-\Delta}^{\Delta} \ldots \int_{-\Delta}^{\Delta} \sum_m \mathrm{e}^{-\kappa\epsilon_m} \mathrm{d}\epsilon_1 \ldots \mathrm{d}\epsilon_N \\
&= \frac{1}{(2\Delta)^N} N \int_{-\Delta}^{\Delta} \ldots \int_{-\Delta}^{\Delta} \mathrm{e}^{-\kappa\epsilon_1} \mathrm{d}\epsilon_1 \ldots \mathrm{d}\epsilon_N \\
&= -\frac{1}{(2\Delta)^N} \frac{N}{\kappa} (2\Delta)^{N-1} \left(\mathrm{e}^{-\kappa\Delta} - \mathrm{e}^{\kappa\Delta}\right) \\
&= \frac{N}{2\kappa\Delta} \left(\mathrm{e}^{\kappa\Delta} - \mathrm{e}^{-\kappa\Delta}\right).
\end{aligned} \tag{8.7}$$

In the second step, we used that each term in the sum gives the same value after the integration and so we can drop the sum against a factor N. But to calculate S, $\langle \ln Z \rangle_\Omega$ is required rather than $\langle Z \rangle_\Omega$. We will now argue that $\langle \ln Z \rangle_\Omega \approx \ln\langle Z \rangle_\Omega$: Consider the partition function of one particular disorder realization ω and write it as the expectation value plus some deviation:

$$Z_\omega = \langle Z \rangle_\Omega + \delta Z_\omega \quad \text{where} \quad \langle \delta Z \rangle_\Omega = 0. \tag{8.8}$$

Assuming $\langle Z \rangle_\Omega \gg \delta Z_\omega$, we can expand the logarithm $\ln(x + \delta x) \approx \ln x + \delta x/x$ and obtain:

$$\langle \ln Z \rangle_\Omega = \langle \ln(\langle Z \rangle_\Omega + \delta Z_\omega) \rangle \approx \ln\langle Z \rangle_\Omega + \left\langle \frac{\delta Z_\omega}{\langle Z \rangle} \right\rangle_\Omega = \ln\langle Z \rangle_\Omega. \tag{8.9}$$

The error of this approximation is of order $(\delta Z/\langle Z \rangle)^2$ and thus small if $\langle Z \rangle$ is large, which is, again, true in the band center, but might not be at the edges.

To get the entropy (8.4), we also have to average the energy E over disorder realizations. But an easier way is to use a relation between E and Z that is well known from thermodynamics:

$$\begin{aligned}
\langle E \rangle_\Omega &= \left\langle -\frac{\partial}{\partial\kappa} \ln Z \right\rangle_\Omega = -\frac{\partial}{\partial\kappa} \langle \ln Z \rangle_\Omega \approx \frac{\partial}{\partial\kappa} \ln\langle Z \rangle_\Omega = -\frac{1}{\langle Z \rangle_\Omega} \frac{\partial}{\partial\kappa} \langle Z \rangle_\Omega \\
&\approx \frac{1}{\kappa} - \Delta \frac{\mathrm{e}^{\kappa\Delta} + \mathrm{e}^{-\kappa\Delta}}{\mathrm{e}^{\kappa\Delta} - \mathrm{e}^{-\kappa\Delta}}.
\end{aligned} \tag{8.10}$$

Using $\langle E \rangle$ and $\langle Z \rangle$, eventually the averaged entropy can be obtained:

$$\langle S \rangle_\Omega = \kappa \langle E \rangle_\Omega + \langle \ln Z \rangle_\Omega \approx 1 - \kappa\Delta \frac{\mathrm{e}^{\kappa\Delta} + \mathrm{e}^{-\kappa\Delta}}{\mathrm{e}^{\kappa\Delta} - \mathrm{e}^{-\kappa\Delta}} + \ln\left(N \frac{\mathrm{e}^{\kappa\Delta} - \mathrm{e}^{-\kappa\Delta}}{2\kappa\Delta}\right). \tag{8.11}$$

These values still depend on the Lagrange parameter $\kappa \in (-\infty, \infty)$. To get the real $\langle S(E) \rangle$ dependence, one should try to eliminate κ, which obviously leads to transcendent equations.

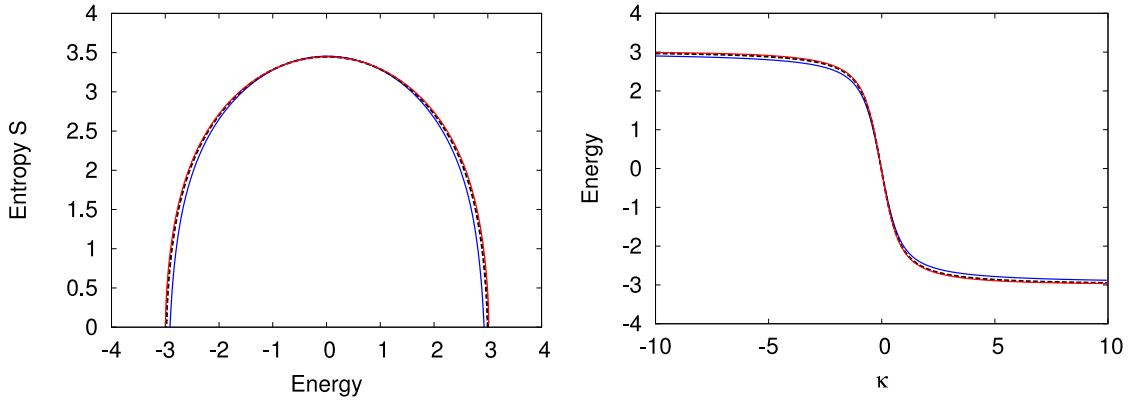

Figure 8.2: Left: Comparison of the entropy of the thermalized state $\langle S(E)\rangle$ obtained by different averaging methods. The red curve represents a numerical averaging over 1,000 disorder realizations. The blue curve is given by equations (8.10) and (8.11) as the results of approximative analytic averages. The black dashed curve represents the result for an equidistant energy distribution. Disorder strength is $W = 4.0$ and lattice size $N = 32$. **Right:** Energy E in dependence of the Lagrange parameter κ (inverse temperature). The colors are different averaging methods as in the left plot. For $\kappa \to \pm\infty$ the band edges are reached, while small κ correspond to energies in the band center.

However, the curve $\langle S(E)\rangle$ is given implicitly from the equations above taking κ as the curve parameter. The last remaining unknown is Δ, the borders of the energy spectrum. In section 2.3.2, an analytical expression for these band edges found by Thouless [Tho74] was presented (2.10). For the disorder strength $W = 4.0$ and coupling strength $A = 1.0$, we find $\Delta(W = 4.0) \approx 3.0$.

To check the quality of the above result, we plotted $S(E)$ parametrically for $N = 32$ and $W = 4.0$ and compared it with the result of numerical averaging. This numerical averaging was done by taking 1,000 disorder realizations, computing the eigenvalues for each realization and then calculating $E(\kappa)$ and $S(\kappa)$. Both were then averaged over the 1,000 realizations resulting in $\langle E(\kappa)\rangle$ and $\langle S(\kappa)\rangle$. Fig. 8.2 shows both curves and they nicely coincide at the band center $-2 < E < 2$. At the band edges, a small deviation is observed which is expected as some of the above approximations are not valid in this region. We conclude that the approximation given by (8.10) and (8.11) is sufficiently good and it will be used later as reference for thermalization.

Additionally, we applied an even simpler approximation for the averaged entropy and energy. This bases on the assumption that the average energy distribution $\{\langle\epsilon_m\rangle\}$ is equidistant: $\langle\epsilon_m\rangle = \epsilon_0 + m \cdot \delta$. For this distribution, E and S can be obtained exactly – see appendix A.2 for calculation details – and the averaging is completely avoided by using this averaged distribution. The results are also shown in Fig. 8.2 and they are also remarkably good – at the band edges even better than the averaging done above. However, we stick to the result from "real" averaging, as its derivation seems more reasonable than assuming an equidistant energy distribution.

We have investigated thermalized states in a linear disordered lattice. The entropy of those states was found to be dependent on the energy. This immediately follows from energy conservation in the system: A state with high energy can only be constructed by mainly exciting

high energy modes, while for states with energies in the band center all eigenmodes can contribute. In the next chapters, it will be investigated if nonlinearity leads to thermalization of the linear lattice by comparing the entropy of a time evolved, initially localized state with the theoretical expectation for thermalized states from above.

9 Numerical Results

9.1 Setup

The numerical simulations were done for short random lattices of different sizes $N = 16, 32, 64$ with periodic boundary conditions. The disorder strength was always $W = 4.0$. The nonlinearity index was set to $\alpha = 1$ (usual DANSE model) and the nonlinear strength was also fixed to $\beta = 1.0$, except for section 9.4. First, we used each eigenmode (delta peaks in eigenmode basis) separately as an initial condition for the simulation. So for each disorder realization, N time evolutions with different initial states were done. Each initial condition corresponds to a different energy and by choosing the eigenmodes, the whole energy spectrum could be reached. Moreover, several disorder realizations were used. The number of realizations was chosen such that in total 256 initial conditions were used for each lattice size N – that is for $N = 16$ we used 16 realizations, for $N = 32$ eight and for $N = 64$ four. The time evolutions were done via the Crank-Nicolson integration scheme (see section 4.4) using a step size of $\Delta t = 0.1$, and we simulated the system up to time $t = 10^7$ (10^8 steps). Additionally, initial single site excitations (delta peaks in position basis) were simulated as well, but only for four disorder realizations for each lattice size N.

At the end of simulation time $t = 10^7$, the entropy in eigenmode representation was computed and averaged over a time window $T = 10^5$. Assuming that the simulation time was large enough to overcome transient motion, this entropy was compared to the expections for thermalized states. The results are presented in the next sections.

9.2 Spectrum Shifting

Before getting to the actual results, one important fact should be mentioned: By diagonalization of the Hamilton operator of a random lattice of size N, one finds N eigenenergies ϵ_m. The disordered potential is chosen uniformly random to have an expected mean value of zero $\langle \overline{V}_\omega \rangle_\Omega = 0$. $\overline{V}_\omega$ here means the mean value for one disorder realization and the average $\langle \cdot \rangle$ is carried out over the realizations. In the limit $N \to \infty$, the mean value for one realization is already zero $\overline{V}_\omega(N \to \infty) = 0$, but for small N, it is not. To ensure a better comparability between different realizations of short lattices, we artificially shifted each potential realization such that its mean value becomes $\overline{V}_\omega = 0$. Technically, the spectrum $\{\epsilon_m\}$ was shifted such that $\bar{\epsilon}_m = 0$, but this is basically the same. This does not change the physics, because any term $\overline{V}\psi_n$ in the DNLS disappears after a transformation $\psi_n \mapsto \psi_n \exp(-i\overline{V}\psi t)$, as already shown in section 4.1. So whenever speaking of energies of a state within these chapters, we implicitly mean the shifted energy according to these considerations.

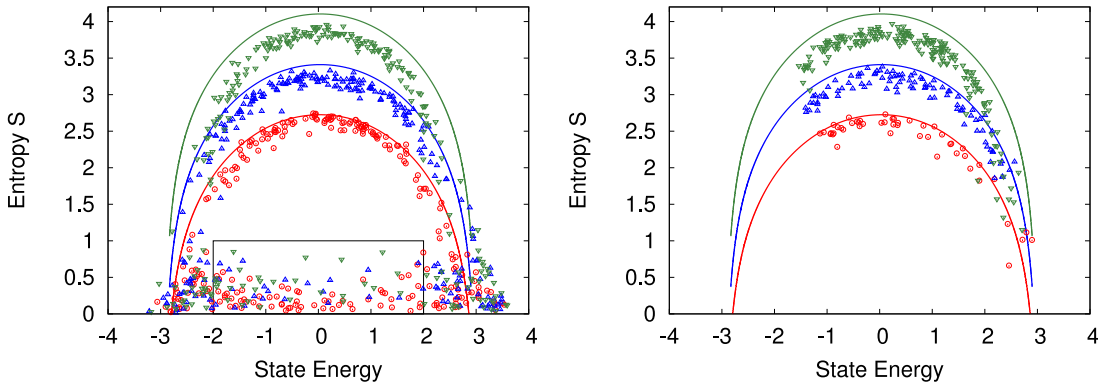

Figure 9.1: Comparison of the entropies from time evolution with the maximal entropies found for the linear chain from thermodynamic arguments. The energies are shifted such that the mean energy $\sum \epsilon_m = 0$ for each disorder realization separately. The points represent the results from the time evolution of the nonlinear problem, while the solid lines are the theoretical results from the averaging given by equations (8.10) and (8.11). Different colors are different lattice sizes: red (bottom) is $N = 16$, blue (middle) is $N = 32$ and green (top) corresponds to $N = 64$. Left plot shows initially excited eigenmodes (peaks in eigenmode base), while on the right initially excited lattice sites (peaks in position base) are shown. The black box on the left indicates the values considered as non thermalized states at the band center. A simple counting gave about 20% - 30% non-thermalized states at the band center.

9.3 Thermalized Entropy

Fig. 9.1 shows the final entropy at $t = 10^7$ for lattice sizes $N = 16$, $N = 32$ and $N = 64$ according to the time evolution of inital eigenmode peaks (left panel) and spatial lattice site peaks (right panel). The solid lines are the analytical results given by equations (8.10) and (8.11). Let us focus on the band center ($-2 < E < 2$) of the left plot first. Many of the initially excited eigenmodes do show high entropies close to the possible maximum for the respective energies (lines). The maximum is not reached exactly due to random fluctuations in the state, but the entropies are reasonably close for being called thermalized. However, there are states in the band center which did not thermalize, indicated by the black box in Fig. 9.1. Their entropy remains low during the whole time evolution up to $t = 10^7$. A simple counting of those states showed that about 20% to 30% of the eigenmodes in the band center did not thermalize.

To our understanding, the non-thermalized modes might be breathers as described in section 4.3.1. Remember that those structures are obtained by continuation of the linear eigenmodes for increasing nonlinearity $\beta > 0$. It seems to happen that some of the eigenmodes induce stable breathers up to $\beta = 1.0$, which are stable, localized objects that can not thermalize. But this is just a conjecture. It is also possible that the non-thermalized modes just have a very long transient motion and will eventually also reach thermalization after a time beyond our simulation.

In contrast, the initially excited lattice sites shown in the right panel exhibited complete thermalization for all states. This supports the theory of breathers, as those are only existing for eigenmodes, but not for excited lattice sites so they cannot appear for excited lattice sites. Note that by exciting single lattice sites, not the whole spectrum width can be reached with

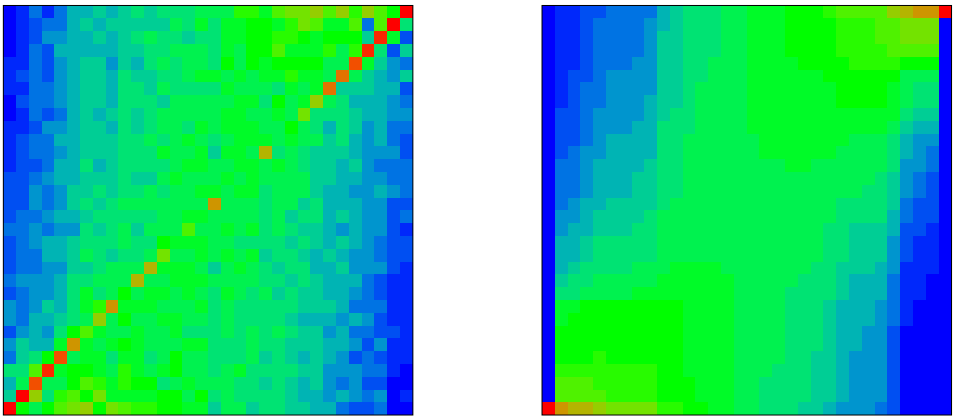

Figure 9.2: Wavefunctions for $N = 32$. Left plot are the wavefunctions obtained from time evolution at time $t = 10^7$. Right plot shows completely thermalized wavefunctions obtained from a Boltzmann distribution for the linear random lattice. Each vertical line represents an averaged wavefunction in eigenmode basis. The y-axis corresponds to the indices of eigenmodes (ordered by their eigenenergy) and each square represents the amount of excitation of this eigenmode $|C_m|^2$ from high (red ≈ 1) to low (blue ≈ 0). The x-axis is the index of the initially excited eigenmode (also ordered by eigenenergy). In the linear case we would just see red squares on the diagonal as the excitation of initial eigenmodes would not change with time. With nonlinearity, as considered, we see that states near the edges of the energy band remain localized (red squares), while states in the band-middle spread across the eigenmodes. Each square represents a wavefunction value averaged over 6 disorder realizations and small time windows. The left plot is obtained using exactly the same realizations and states as in Fig. 9.1

the initial energies. The asymmetry of the points comes from the nonlinear term, which shifts the energy by $\beta/2$ for lattice site peaks.[1]

Fig. 9.2 shows the wavefunctions at time $t = 10^7$ as density plots (left) compared to Boltzmann distributions (right). Without nonlinearity, the left plot would just show red squares on the diagonal while everything else would be blue. But due to nonlinearity, the states spread and the plot looks similar to the right one where Boltzmann distributions as completeley thermalized wavefunctions are shown. The entropies of those Boltzmann distributions are located on the lines in Fig. 9.1. Comparing the two density plots left and right, one recognizes similarities in the band center. Despite some remaining peaks, most of the eigenmodes spread out and thermalize indicated by the green region in the center similar to the appearance for the Boltzmann distributions. This is consistent with the results from Fig. 9.1 indicating thermalization for a majority of eigenmodes.

9.4 Fraction of Thermalized States

In the preceding section, we saw that a fraction of the eigenmodes did not thermalize during our integration and we interpreted this with the existence of breathers in the lattice. Now the natural question to ask would be if and how this fraction depends on the nonlinear strength β.

[1] For excited eigenmodes, the nonlinear energy is usually smaller than $\lesssim \beta/10$ and so we do not see those effects as clearly in the left plot.

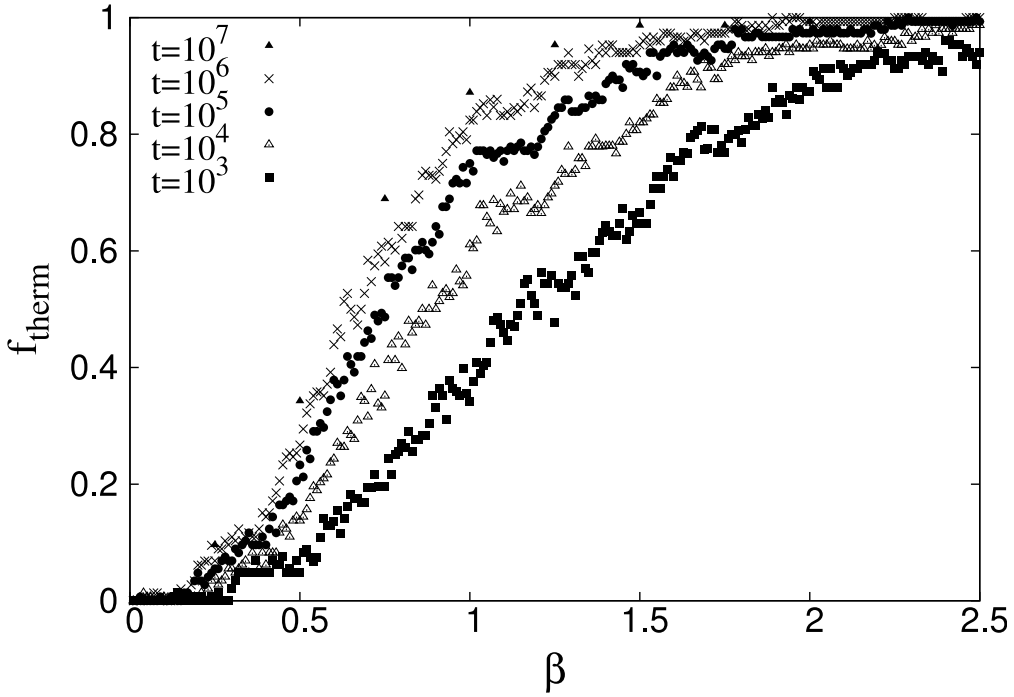

Figure 9.3: Fraction of thermalized states $f_{\text{therm}} = N_{\text{therm}}(t)/N_{\text{center}}$ against the nonlinear strength β for different times t. Lattice size again was $N = 32$ and disorder strength $W = 4.0$. Like before, all eigenmodes were chosen as initial conditions for eight disorder realizations, but time evolution was done for many values of β this time. For the data analysis, only states with energy in the band center $|E| < 2$ contributed, where those with entropy $S > 1$ after time t were considered as being thermalized (compare box in Fig. 9.1). As expected, the number of thermalized states grows for increasing nonlinear strength and also for increasing time t. (Graph created by Karsten Ahnert)

This was addressed by another simulation. Again, we used a lattice of size $N = 32$ with eight disorder realization of the random potential and with the disorder strength $W = 4.0$. The nonlinear strength β was ranged from $0 \ldots 2.5$ and for each β the time evolution of initially excited eigenmodes were obtained. But this time only those eigenmodes lying in the band center $-2 < E < 2$ were considered. At times $t = 10^3, 10^4, 10^5, 10^6$ and 10^7 the fraction of thermalized states $f_{\text{therm}} = N_{\text{therm}}(t)/N_{\text{center}}$ was computed. N_{center} is the total number of eigenmodes in the band center and $N_{\text{therm}}(t)$ is the number of states having an entropy $S > 1$ at time t, which we interpreted as thermalized states.

The results of these simulations are shown in Fig. 9.3. As one naturally expects, f_{therm} increases with both β and time t. This is consistent with the breather conjecture. For larger nonlinearity, less breathers should exist and more modes should thermalize. We found that for $\beta \lesssim 0.2$ almost no states thermalized at all even for $t = 10^7$ and for $\beta \gtrsim 2.2$ nearly all states thermalized already at $t = 10^5$. For values of β between those borders, the fraction of thermalized states shows a clear increase with time. Unfortunately, our simulation does not show a saturation of this increase, but we suspect such a saturation curve $f_{\text{therm}}(\beta, t \to \infty)$ to exist and from the relatively small increase from $t = 10^6$ to $t = 10^7$ we conclude that it should not be far from the points at 10^7.

9.5 Thermalization at the Band Edges

In the band center, the entropy is very useful to distinguish between thermalized and non-thermalized states. However, on the band edges, the maximal entropy is so low that a determination of thermalized states is hardly possible. Anyhow, to learn something about those states as well, additional numerical simulations under slightly different conditions were carried out. We again used short disordered lattices of size $N = 32$, but started only with an excitation of the second eigenmode, that is, the mode with second lowest energy.[2] Now, thermalization is measured by means of the excitation of the *first* eigenmode $|C_1|^2$. That is reasonable because a thermalized state would have $|C_1|^2 \gtrsim |C_2|^2$. So we initialized with $|C_2|^2 = 1$, simulated up to $t = 10^7$ and then checked the excitation $|C_1|^2$ – this was done for 265 different disorder realizations. From simple perturbation theory for two nonlinear coupled oscillators (C_1 and C_2), one would expect $|C_1|^2 \sim (V_{1222})^2$, as this is the highest order coupling term that can induce probability transfer. Note that the coupling term V_{1122} does not induce probability flows as shown in appendix A.3.

The result of the simulation is shown in Fig. 9.4. We considered states to be thermalized if $|C_1|^2 \approx 1$ (black box), while states close to the expectation from perturbation theory are not thermalized. The dashed line simply shows the slope $(V_{1122})^2$ as a guide to the eye. Qualitatively, the situation is similar to the one in the band center: some states did thermalize (black box in the graph), while others did not. In contrast to the band center, non-thermalizing states are the majority at the band edges: more than 80% of the initial modes did not thermalize within integration time. To stress the breather explanation again, that can be understood by keeping in mind that high energy modes have short localization lengths which makes them generally more stable than modes in the band center. From Fig. 9.4, one also can conclude that modes with larger overlap V_{1222} are more likely to thermalize than those with small overlaps. But the large amount of states lying between the two cases leads to the suspicion that our simulation time was to short. Many states are still "on the way" to thermalization – that means the thermalization progress is much slower at the band edges than in the center.

To our understanding, the main result from this simulation is that states at the band edges can thermalize, too. However, a quantitative measurement on the number of non-thermalized states was not really possible as it requires for longer integration time.

[2] Note, that β was 1.0, thus positive, which shifts the energy of the initial state more towards the band center and not out of the spectrum.

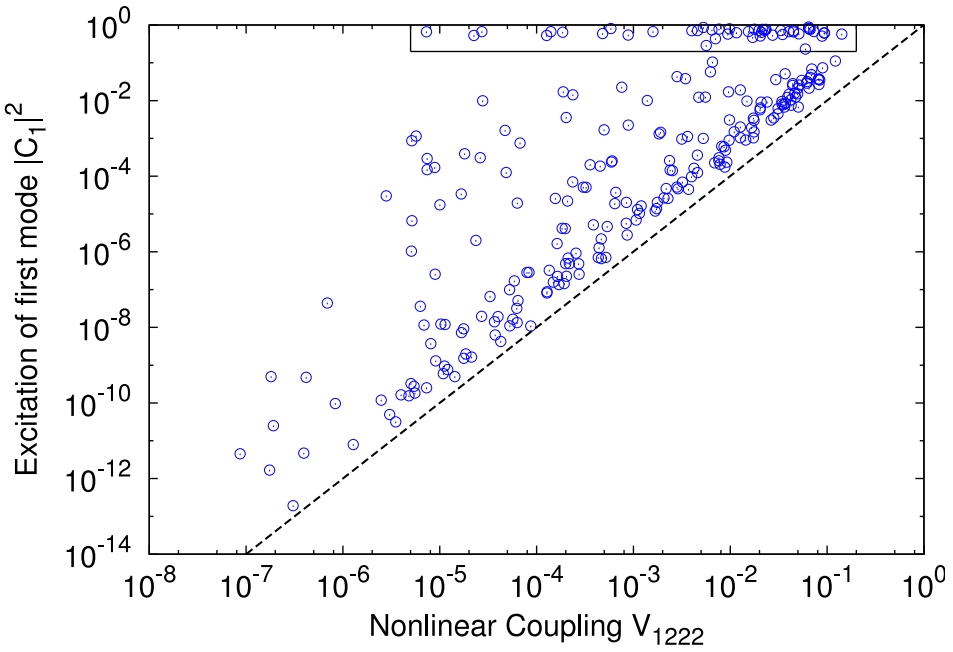

Figure 9.4: Thermalization at the edge of the energy band. The excitation of the the first mode $|C_1|^2$ at time $t = 10^7$ is plotted vs. the nonlinear coupling strength V_{1222}. Each point represents a time evolution of an initially excited second mode (second lowest energy value in the spectrum) for a different disorder realization of length $N = 32$ and fixed $\beta = 1.0$. In total, 256 realizations were simulated resulting in 256 points in this figure. The dotted line is a simple $(V_{1222})^2$ graph representing the expected results for two coupled nonlinear oscillators with coupling strength V_{1222}. Points close to that line are not thermalized in our sense, while points with $|C_1|^2 \approx 1$ are. The black box at the top indicates the states which we considered to be thermalized (states with $|C_1|^2 \gtrsim 0.5$). We see that even for very small coupling, thermalization is reached for some disorder realizations. The number of thermalized states increases with increasing strength of the coupling, but in total a much smaller fraction of states seems to thermalize at the band edges than in the band center. So we found only 40 of 256 states ending up thermalized after $t = 10^7$, while in the center about 70 of 100 states exhibit thermalization

Part IV

Summary and Conclusions

Summary

In part II, a generalized version of the DANSE model with a new parameter α – the nonlinearity index – was investigated. Former results on the spreading exponent $\gamma \approx 0.30 - 0.35$ were recapitulated for initially localized wavefunctions. A derivation for the spreading exponent in the generalized DANSE model was presented and the results were compared with numerical runs showing good correspondence with the assumptions of "weak" and "very weak" stochasticity. Overall, the spreading behavior for different nonlinear indices followed our expectations. The mathematical considerations using a nonlinear diffusion equation seems fruitful. However, there still remain some unclear aspects about the spreading mechanisms. The exact relation between a and α found by the numerical simulations is not yet understood completely. It might be, that the downscaling supposed by Flach et al. is induced by a decrease of chaoticity during the spreading which might lead to a spreading exponent according to the "very weak" stochasticity. More research on this is required for more understanding of the interplay between disorder and nonlinearity.

Furthermore, the structural entropy S_{str} as a measure for the peak structure of probability distributions was introduced. Numerical simulations on S_{str} for spreading wavefunctions in disordered lattices showed that their peak structure remains unchanged. Hence, the spreading mechanism does not prefer peaks nor background noise, but preserves the complex structural properties of the wavefunctions. This result is not surprising, but still remarkable, as, to our knowledge, structural properties of wavefunctions in this setup have not been studied up to now.

In part III, thermalization in short disordered nonlinear lattices was numerically investigated for the usual DANSE model ($\alpha = 1$). Thermalization was defined by maximization of the entropy. Analytical results on the energy dependence of the entropy of thermalized states were obtained and good approximations for averages over disorder realizations could be found. The energy dependence of spreading was investigated numerically and the results were compared to the analytical approximations. It was found that most of the states with energy in the band center do thermalize. Those which don't are believed to be breather solutions that don't spread at all and their number depends on the nonlinear strength β. Above a critical value of nonlinear strength, complete thermalization was observed while below another critical nonlinear strength, no thermalization at all took place. It was also found that states near the edges of the energy band are more likely to not thermalize compared with those close to the band center. Furthermore, the thermalization process itself is much slower, which comes from the smaller localization length of the high energetic modes.

Note that thermalization implies spreading as a state that does not thermalize also remains spatially localized due to the localized character of the eigenmodes. From the fact that close to the edges of the energy band the thermalization is slow and rare, we conclude that states in this energy regime would also hardly spread in large lattices. Initial conditions in the center of the energy band, on the other hand, do show thermalization and hence, they should also exhibit spreading in large lattices. However, our simulations with initially excited lattice sites always showed thermalization, which means that position peaks should always spread in large lattices as well.

Outlook

For further knowledge about the spreading in the gDANSE model, a closer investigation of the mechanisms of diffusion seems required. One could, for example, try to observe the spreading in eigenmode base, but the numerical effort would be huge as the basis-transformations are quite expensive in terms of computation time. Another idea could be to calculate finite time Lyapunov exponents during the spreading which might lead to an explanation of the downscaling by showing a reducing chaoticity.

Additionally, a detailed analyzation of the breather solution and their stability might give more insights on the fraction of thermalized states observed in short lattices. Also the behavior for different lattice sizes and disorder strengths could be of interest. It would also be interesting to investigate the relation between thermalization and spreading by analyzing the spreading behavior of high energy modes in large lattices. Furthermore, thermalization for different nonlinear indices α should be studied and compared with the spreading results. Our findings on thermalization may also provide a link to the scattering problem [TP08] and the question of thermoconductivity in disordered chains. Further numerical simulations on this topic are planned.

A Mathematical Calculations

A.1 gDANSE in Eigenmode Representation

Starting with the generalized Discrete Anderson Nonlinear Schrödinger Equation (gDANSE) in normal position representation (dots mean time derivatives):

$$i\dot{\psi}_n = V_n\psi_n + \psi_{n-1} + \psi_{n+1} + \beta|\psi_n|^{2\alpha}\psi_n, \tag{A.1}$$

we introduce eigenmodes of the linear part $\phi_{m,n}$ where m is the index of the eigenfunction and n is the spatial index. So $\phi_{m,n}$ is the complex value of the m-th eigenfunction at lattice site n. The eigenmodes form a basis and accordingly, they are orthonormal

$$\sum_n \phi_{m,n}\phi^*_{m',n} = \delta_{mm'}, \tag{A.2}$$

and are defined to solve the time independent, linear eigenvalue problem:

$$V_n\phi_{m,n} + \phi_{m,n-1} + \phi_{m,n+1} = \epsilon_m\phi_{m,n}. \tag{A.3}$$

We can now expand the values ψ_n into this eigenmode basis

$$\psi_n = \sum_m C_m\phi_{m,n}, \tag{A.4}$$

with expansion coefficients C_m. We will now derive an equation for the time dependence of the C_m by substituting the expansion (A.4) into the gDANSE (A.1):

$$\begin{aligned} i\sum_m \dot{C}_m\phi_{m,n} = {} & V_n\sum_m C_m\phi_{m,n} + \sum_m C_m\phi_{m,n-1} + \sum_m C_m\phi_{m,n+1} \\ & + \beta\,\Big|\sum_m C_m\phi_{m,n}\Big|^{2\alpha}\cdot\sum_m C_m\phi_{m,n} \\ = {} & \sum_m C_m(\underbrace{V_n\phi_{m,n} + \phi_{m,n-1} + \phi_{m,n+1}}_{=\epsilon_m\phi_{m,n}}) + \beta\,\Big|\sum_m C_m\phi_{m,n}\Big|^{2\alpha}\cdot\sum_m C_m\phi_{m,n}. \end{aligned}$$

Now we multiply both sides of the equation by $\phi^*_{m',n}$ from the right and apply a summation over the spatial index n. From the orthonormalization of the eigenmodes (A.2), the linear part of the equation becomes trivial:

$$i\dot{C}_{m'} = \epsilon_{m'}C_{m'} + \beta\underbrace{\sum_n\left[\Big|\sum_m C_m\phi_{m,n}\Big|^{2\alpha}\phi^*_{m',n} + \sum_m C_m\phi_{m,n}\phi^*_{m',n}\right]}_{=:S}. \tag{A.5}$$

As expected, the linear term produces a linear phase growth $C_m \sim \exp(i\epsilon_m)$, while the nonlinear on-site potential is transformed to a rather complicated nonlinear multi-mode coupling.

This coupling term, named S here, has to be investigated further. We expand the absolute square to a product of complex conjugates, change the indices $m \to \widehat{m},\ \widetilde{m},\ \bar{m}$ in the remaining summations and replace m' with m.

$$S = \sum_n \left[\left(\sum_{\widehat{m}} C_{\widehat{m}} \phi_{\widehat{m},n} \right)^{\alpha} \cdot \left(\sum_{\widetilde{m}} C^*_{\widetilde{m}} \phi^*_{\widetilde{m},n} \right)^{\alpha} \cdot \left(\sum_{\bar{m}} C_{\bar{m}} \phi_{\bar{m},n} \phi^*_{m,n} \right) \right].$$

Now the terms with power α can be written as product of α summations:

$$\left(\sum_{\widehat{m}} C_{\widehat{m}} \phi_{\widehat{m},n} \right)^{\alpha} = \left(\sum_{\widehat{m}_1} C_{\widehat{m}_1} \phi_{\widehat{m}_1,n} \right) \cdots \left(\sum_{\widehat{m}_\alpha} C_{\widehat{m}_\alpha} \phi_{\widehat{m}_\alpha,n} \right),$$

and accordingly for the second term with $\widetilde{m}$. If this is reentered into the above equation, we can reorganize and combine the summations obtaining:

$$S = \sum_{\substack{\widehat{m}_1 \ldots \widehat{m}_\alpha \\ \widetilde{m}_1 \ldots \widetilde{m}_\alpha \\ \bar{m}}} V^{\widehat{m}_1 \ldots \widehat{m}_\alpha}_{\widetilde{m}_1 \ldots \widetilde{m}_\alpha \, \bar{m},m} C_{\widehat{m}_1} \cdots C_{\widehat{m}_\alpha} \cdot C^*_{\widetilde{m}_1} \cdots C^*_{\widetilde{m}_\alpha} C_{\bar{m}}, \tag{A.6}$$

where the $(2\alpha + 2)$ – eigenmode overlap integral V is introduced:

$$V^{\widehat{m}_1 \ldots \widehat{m}_\alpha}_{\widetilde{m}_1 \ldots \widetilde{m}_\alpha \, \bar{m},m} := \sum_n \phi_{\widehat{m}_1,n} \cdots \phi_{\widehat{m}_\alpha,n} \cdot \phi^*_{\widetilde{m}_1,n} \cdots \phi^*_{\widetilde{m}_\alpha,n} \phi_{\bar{m},n} \cdot \phi^*_{m,n}. \tag{A.7}$$

It has to be noted that the reorganization done in this last step is only allowed for finite summations and this calculation is thus restricted to finite lattices.[1] Eventually, the equations of motions for the eigenmode coefficients $C_m(t)$ are:

$$i\dot{C}_m = \epsilon_m C_m + \beta S = \epsilon_m C_m + \sum_{\substack{\widehat{m}_1 \ldots \widehat{m}_\alpha \\ \widetilde{m}_1 \ldots \widetilde{m}_\alpha \\ \bar{m}}} V^{\widehat{m}_1 \ldots \widehat{m}_\alpha}_{\widetilde{m}_1 \ldots \widetilde{m}_\alpha \, \bar{m},m} C_{\widehat{m}_1} \cdots C_{\widehat{m}_\alpha} \cdot C^*_{\widetilde{m}_2} \cdots C^*_{\widetilde{m}_\alpha} C_{m'}. \tag{A.8}$$

For the usual choice $\alpha = 1$, the equation takes a simpler form with only 3 summation indices:

$$i\dot{C}_m = \epsilon_m C_m + \beta \sum_{\widehat{m},\widetilde{m},m'} V_{\widehat{m},\widetilde{m},m',m} C_{\widehat{m}} C^*_{\widetilde{m}} C_{m'}, \tag{A.9}$$

where $V_{\widehat{m},\widetilde{m},m',m}$ is the 4-wavefunction overlap according to (A.7).

Note that the above calculation seems to demand $\alpha \in \mathbb{N}^+$, but we only need $(2\alpha + 2) \in \mathbb{N}^+$ to ensure an integer valued number of indices in (A.8). So $\alpha = 0.5$ as used in numerical simulations is not causing problems here.

[1] From the exponentially localized character of the eigenmodes ϕ_m it is surely possible to argue that the infinite summation can be truncated because the remaining terms are exponentially small and the argumentation also should hold for infinite lattices.

A.2 Entropy of Equidistant Energy Levels

Suppose we have a system with N energy levels E_n in the interval $-\Delta/2 \dots \Delta/2$ with constant spacing $\delta = \Delta/(N-1)$:

$$E_n = -\frac{\Delta}{2} + n \cdot \frac{\Delta}{N-1} = E_0 + n\delta, \quad n = 0 \dots N-1, \tag{A.10}$$

where we introduced the lower boundary of the spectrum $E_0 = -\Delta/2$ for simplicity. Moreover, suppose the system is populated by one particle spread across all energies. The probability to find the particle in level n is defined to be p_n, where normalization $\sum p_n = 1$ should hold. It is well known that the entropy, defined as

$$S = -\sum_{n=0}^{N-1} p_n \ln p_n \tag{A.11}$$

reaches its maximal value for the Boltzmann (or Gibbs) distribution

$$p_n = \frac{1}{Z} \mathrm{e}^{-\beta E_n}, \tag{A.12}$$

where β is the Lagrange parameter connected with energy conservation and is usually interpreted as the inverse temperature. Z ensures normalization and thus can be computed as:

$$\begin{aligned} Z(\beta) &= \sum_{n=0}^{N-1} \mathrm{e}^{-\beta E_n} = \sum_{n=0}^{N-1} \mathrm{e}^{-\beta(E_0+n\delta)} = \mathrm{e}^{-\beta E_0} \sum_{n=0}^{N-1} (\mathrm{e}^{-\beta\delta})^n \\ &= \mathrm{e}^{-\beta E_0} \frac{1-\mathrm{e}^{-\beta N\delta}}{1-\mathrm{e}^{-\beta\delta}} = \frac{e^{\beta\delta N/2} - \mathrm{e}^{-\beta\delta N/2}}{e^{\beta\delta/2} - \mathrm{e}^{-\beta\delta/2}}. \end{aligned} \tag{A.13}$$

It is called the partition function. In the last step we substituted $E_0 = -\delta(N-1)/2$. The energy of a Boltzmann distribution can be computed as follows

$$\begin{aligned} E(\beta) &= \sum_{n=0}^{N-1} p_n E_n = \frac{\mathrm{e}^{-\beta E_0}}{Z} \sum_{n=0}^{N-1} (E_0 + n\delta)\mathrm{e}^{-\beta n\delta} \\ &= E_0 + \frac{\delta \mathrm{e}^{-\beta E_0}}{Z} \sum_{n=0}^{N-1} n(\mathrm{e}^{-\beta\delta})^n \\ &= E_0 + \frac{\delta \mathrm{e}^{-\beta E_0}}{Z} \frac{(N-1)\mathrm{e}^{-\beta(N+1)\delta} - N\mathrm{e}^{-\beta\delta}(1-\mathrm{e}^{-\beta N\delta})}{(\mathrm{e}^{-\beta\delta}-1)} \\ &\overset{(A.13)}{=} E_0 - \frac{\delta}{1-\mathrm{e}^{-\beta N\delta}} \frac{(N-1)\mathrm{e}^{-\beta(N+1)\delta} - N\mathrm{e}^{-\beta N\delta} + \mathrm{e}^{-\beta\delta}}{\mathrm{e}^{-\beta\delta}-1} \\ &= E_0 - \delta\left(\frac{N\mathrm{e}^{-\beta N\delta}}{1-\mathrm{e}^{-\beta N\delta}} + \frac{\mathrm{e}^{\beta\delta}}{\mathrm{e}^{-\beta\delta}-1}\right) \\ &= E_0 + \delta\left(\frac{N}{1-\mathrm{e}^{\beta N\delta}} + \frac{1}{\mathrm{e}^{\beta\delta}-1}\right) \\ &= \frac{\Delta}{N-1}\left(\frac{N}{1-\mathrm{e}^{\beta N\delta}} + \frac{1}{\mathrm{e}^{\beta\,\delta}-1}\right) - \frac{\Delta}{2}. \end{aligned} \tag{A.14}$$

Using these results, the entropy gives

$$\begin{aligned} S(\beta) = & -\sum_{n=0}^{N-1} p_n \ln p_n = -\frac{1}{Z} - \sum_{n=0}^{N-1} \mathrm{e}^{-\beta E_n} (\ln \mathrm{e}^{-\beta E_n} - \ln Z) \\ & = \beta E + \ln Z \\ & = \frac{\beta\Delta}{N-1} \left(\frac{N}{1-\mathrm{e}^{\beta\delta N/(N-1)}} + \frac{1}{\mathrm{e}^{\beta\delta/(N-1)}-1} \right) \\ & \quad + \ln\left(1-\mathrm{e}^{-\beta\Delta N/(N-1)}\right) - \ln\left(1-\mathrm{e}^{-\beta\Delta/(N-1)}\right). \end{aligned} \tag{A.15}$$

Thus, for each $\beta \in (-\infty, \infty)$ [2] a corresponding energy and entropy can be calculated from equations (A.14) and (A.15). This implicitly gives the relation between energy and entropy $S(E)$ depending on the width of the energy spectrum Δ and the number of energy levels N.

A.3 Probability Flow for Symmetric Coupling

Here, it will be briefly shown that the symmetric coupling term V_{1122} in the DANSE equation in eigenmode representation can not lead to a probability flow between two oscillators. We start with the DANSE in eigenmode base (4.1) for two lattice sites and take only the coupling term V_{1122} into consideration and set $\beta = 1.0$. Assuming that only the second oscillator is initially excited $C_2 = 1$, $C_1 = 0$, the equation of motion for C_1 reads:

$$i\dot{C}_1 = \epsilon_1 C_1 + V_{1122} C_1 C_2 C_2^*. \tag{A.16}$$

From this, the time derivative of the norm $|C_1|^2$ can be computed:

$$\begin{aligned} \frac{\mathrm{d}}{\mathrm{d}t}|C_1|^2 &= \dot{C}_1^* C_1 + C_1^* \dot{C}_1 = -i(\epsilon_1 C_1^* + V_{1122} C_1^* C_2^* C_2) C_1 + i(\epsilon_1 C_1 + V_{1122} C_1 C_2 C_2^*) C_1^* \\ &= i(\epsilon_1 |C_1|^2 + V_{1122} |C_1|^2 |C_2|^2) - i(\epsilon_1 |C_1|^2 + V_{1122} |C_1|^2 |C_2|^2) \\ &= 0 \end{aligned}$$

So no probability will be transferred via the symmetric coupling term V_{1122}.

[2] β can be negative as we have negative energies in our system.

B Spreading Exponent

In this chapter, the calculations of Flach et al. [FKS09] on the spreading law are recapitulated in a generalized form for the gDANSE model. At first, arguments assuming highly chaotic modes are shown and then some reasons for the downscaling are presented. The results are equivalent to the cases of strong and very weak stochasticity given in section 7.1.

B.1 Highly Chaotic Modes

Again, it is convenient to use the basis of localized eigenmodes from eq. (4.5) for calculation. First of all, note that if a state is spatially spread over, say, Δn lattice sites, then from the localized character of the eigenmodes, it is very natural to assume it is also spread across roughly Δn eigenmodes. Moreover, it is possible to assign a spatial index to each eigenmode, e.g. by taking its highest peak or the position expectation value. In the following, we assume that the eigenmodes are ordered spatially, that is eigenfunction m and $m \pm 1$ are localized at neighboring lattice sites, which on the other hand means that their energy distance is random and generally of the order of half the spectrum width.

So imagine a state C_m being spread over Δn sites/eigenmodes and the plateau, which we assume of rectangular shape, is starting at eigenmode m^*. Thus, we have the following situation: $C_m \approx 0$ for $m \leq m^*, m > m^* + \Delta n$ and $|C_m| \approx 1/\sqrt{\Delta n}$ for $m^* < m < m^* + \Delta n$. We completely neglected phases which are assumed to be random for this ansatz. This assumption would be true if all modes show chaotic behavior. Now we are interested in the time evolution of the m^*-th eigenmode as given by the gDANSE:

$$i\dot{C}_{m^*} = \epsilon_{m^*} C_{m^*} + \beta \sum_{\substack{\widehat{m}_{1\ldots\alpha} \\ \widetilde{m}_{1\ldots\alpha} \\ m'}} V^{\widehat{m}_{1\ldots\widehat{m}_\alpha}}_{\widetilde{m}_{1\ldots\widetilde{m}_\alpha} \; m',m^*} C_{\widehat{m}_1} \cdots C_{\widehat{m}_\alpha} C^*_{\widetilde{m}_1} \cdots C^*_{\widetilde{m}_\alpha} C_{m'}. \tag{B.1}$$

Again, from the localization of the eigenmodes, we find that the overlap V drops exponentially with increasing spatial distance of the modes, thus also with increasing distances of the index values. The most dominant term in the sum above is the one with all indices $\widehat{m}_{1\ldots\alpha} = \widetilde{m}_{1\ldots\alpha} = m' = m^* + 1$. So we get, dropping constant factors and using m instead of m^*, the following relation for $\dot{C}_m$

$$i\dot{C}_m \sim (C_{m+1} C^*_{m+1})^\alpha C_{m+1}.$$

Taking the modulus of both sides and using $|C_{m+1}| \approx 1/\sqrt{\Delta n}$ we obtain

$$|i\dot{C}_m| \sim (\Delta n)^{-(\alpha+1/2)}. \tag{B.2}$$

This leads to an excitation of the exterior mode C_m as following:

$$|C_m|^2 \sim (\Delta n)^{-(2\alpha+1)} t. \tag{B.3}$$

From this, the momentary diffusion rate D can be calculated from the inverse time that is needed to excite mode m up to the plateau $|C_m(T)|^2 \approx 1/\Delta n$:

$$D = 1/T \sim (\Delta n)^{-2\alpha}. \tag{B.4}$$

If we finally take the diffusion equation $(\Delta n)^2 \sim Dt$ we end up at an estimation for the time dependence of Δn:

$$(\Delta n)^2 \sim t^{\gamma_T}, \quad \text{with} \quad \gamma_T = \frac{1}{\alpha + 1}. \tag{B.5}$$

For the usual case $\alpha = 1$, (B.5) recapitulates the result found in [FKS09], which was $\gamma_T = 0.5$. This is equivalent to the case of "strong stochasticity" discussed in section 7.1. Unfortunately, previous numerical simulations disagree with this result as a spreading exponent of $\gamma_{\text{numerics}} \approx 0.35$ was found, see [PS08, She93] for example.

B.2 Downscale of Spreading

To get a better description of the numerical results, Flach et al. presented some calculations assuming the existence of non-chaotic modes which do not contribute to the spreading resulting in a downscale of the spreading law [FKS09]. The existence of those modes is supported by numerical results shown in Fig. B.1. This plot was obtained from our own numerics, which closely follow those from Flach.

Consider a wavefunction plateau of size Δn with average excitation $|C_m|^2 \approx 1/(\Delta n)$. Formally, we can use a perturbation approach to the gDANSE and find that this normal mode will excite other modes $C_{m'}$ in first order as:

$$|C_{m'}| = \beta(\Delta n)^{-\alpha} R^{-1}_{m,m'} |C_m|, \qquad R_{m,m'} \sim \left| \frac{\epsilon_m - \epsilon_{m'}}{V_{m',m\ldots m}} \right|. \tag{B.6}$$

$V_{m',m\ldots m}$ means all $2\alpha{+}2$ index values of V are m, except the first one.Now if $R_{m,m'} < \beta(\Delta n)^{-\alpha}$ the perturbation approach breaks down and resonances set in resulting in chaotic motion. To find out how often, if at all, this might happen, a numerical analysis was performed. Again following the ideas of [FKS09] we obtained $R_{m,\min} = \min_{m' \neq m}\{R_{m,m'}\}$ for each eigenmode of a lattice of size $N = 1024$. To improve statistics, we repeated this for 1,000 different disorder realizations and found a probability distribution $w(R_{m,\min})$ which is shown in fig. B.1 for different nonlinear indices α. In agreement to [FKS09] we found that $w(R_{\nu,\min} \to 0) \to B(\alpha) \neq 0$. Furthermore, the probability $\mathcal{P}$ for a mode excited to the level $1/(\Delta n)$ to be in resonance with (at least) one other mode is

$$\mathcal{P} = \int_0^{\beta(\Delta n)^{-\alpha}} \mathcal{P}(x)\mathrm{d}x. \tag{B.7}$$

For $\beta(\Delta n)^{-\alpha} \ll 1$ it follows that

$$\mathcal{P} \approx B(\alpha)\beta(\Delta n)^{-\alpha}, \tag{B.8}$$

which can also be understood as the average fraction of chaotic modes in the plateau. Assuming that only this fraction shows chaotic motion and contributes to further excitation,

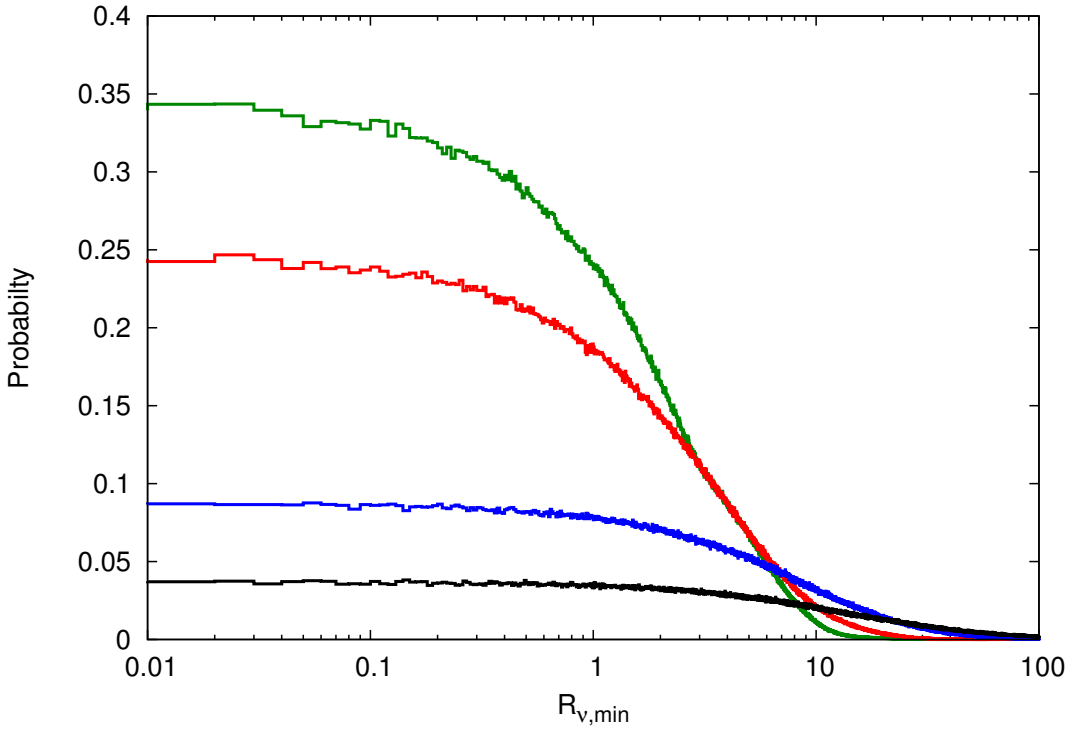

Figure B.1: Probability distribution for resonances of eigenmodes $\mathcal{P}(R_{\nu,\min})$ for different nonlinear indices $\alpha = 0.5$, $\alpha = 1$, $\alpha = 2$, $\alpha = 3$ (order top to bottom) and $W = 4$. Main result is that $\mathcal{P}(R_{\nu,\min} \to 0) \to B(\alpha) \neq 0$.

we correct eqn. (B.3) and find that exterior modes are excited as

$$|C_m|^2 \sim (\Delta n)^{-(4\alpha+1)} t. \tag{B.9}$$

Similar calculations as presented in appendix B.1 lead to a new spreading law:

$$(\Delta n)^2 \sim t^{\gamma_n}, \quad \text{with} \quad \gamma_n = \frac{1}{2\alpha+1}. \tag{B.10}$$

We, again, want to note that this reasoning is arguable. As a matter of fact, we are not convinced by the explanation which states the existence of non-chaotic modes within the spreading plateau of the wavefunction. It seems very unnatural to assume some mode excitations C_m behave regularly while the surrounding ones are chaotic. It's also unclear why the "unchaotic" modes can get excited by chaotic excitations and then show regular motion.

Bibliography

[And58] P. W. Anderson, *Absence of diffusion in certain random lattices*, Physical Review Letters **109** (1958), no. 5, 1492–1505.

[Aub97] Serge Aubry, *Breathers in nonlinear lattices: Existence, linear stability and quantization*, Physica D **103** (1997), 201–250.

[bac99] Thorsten Fließbach, *Statistische physik*, Spektrum Akad. Verlag Heidelberg, Berlin, 1999.

[BMRF+99] D. Boiron, C. Mennerat-Robilliard, J.-M. Fournier, L. Guidoni, C. Salomon, and G. Grynberg, *Trapping and cooling cesium atoms in a speckle field*, The European Physical Journal D **7** (1999), no. 3, 373–377.

[Bor63] R. E. Borland, *The nature of the electronic states in disordered one-dimensional systems*, Proceesings of the Roy. Soc. A **274** (1963), 529–545.

[BS93] C. Beck and F. Schlögel, *Thermodynamics of chaotic systems*, Cambridge Universityc Press, 1993.

[CLG+08] Julien Chabé, Gabriel Lemarié, Benoît Grémaud, Dominique Delande, Pascal Szriftgiser, and Jean Claude Garreau, *Experimental observation of the Anderson metal-insulator transition with atomic matter waves*, Physical Review Letters **101** (2008), no. 25, 255702.

[CPV93] A. Crisanti, G. Paladin, and A. Vulpiani, *Products of random matrices in statistical physics*, Springer-Verlag, 1993.

[CVH+05] D. Clément, A. F. Varón, M. Hugbart, J. A. Retter, P. Bouyer, L. Sanchez-Palencia, D. M. Gangardt, G. V. Shlyapnikov, and A. Aspect, *Suppression of transport of an interacting elongated Bose-Einstein condensate in a random potential*, Physical Review Letters **95** (2005), no. 17, 170409.

[DGPS99] F. Dalfovo, S. Giorgini, L. P. Pitaevskii, and S. Stringari, *Theory of Bose-Einstein condensation in trapped gases*, Review of Modern Physics **71** (1999), 463–512.

[EJ03] J. C. Eilbeck and M. Johansson, *The discrete nonlinear schrödinger equation – 20 years on*, Zorzano (Eds.), Proceedings of the Third Conference on Localization and Energy Transfer in Nonlinear Systems, June 17–21, 2003, pp. 44–67.

[FFG+05] C. Fort, L. Fallani, V. Guarrera, J. E. Lye, M. Modugno, D. S. Wiersma, and M. Inguscio, *Effect of optical disorder and single defects on the expansion of a Bose-Einstein condensate in a one-dimensional waveguide*, Physical Review Letters **95** (2005), no. 17, 170410.

[FFI08] Leonardo Fallani, Chiara Fort, and Massimo Inguscio, *Bose-Einstein condensates in disordered potentials*, arXiv:0804.2888v2 [cond-mat.dis-nn] (2008).

[FKS09] S. Flach, D. O. Krimer, and Ch. Skokos, *Universal spreading of wave packets in disordered nonlinear systems*, Physical Review Letters **102** (2009), no. 2, 024101.

[HT99] D. Hennig and G. P. Tsironis, *Wave transmission in nonlinear lattices*, Physics Reports **307** (1999), no. 5-6, 333–432.

[HT01] P. Harremoës and F. Topsøe, *Inequalities between entropy and index of coincidence from information diagrams*, IEEE Trans. Inform. Theory **47** (2001), no. 2944.

[JBC+98] D. Jaksch, C. Bruder, J. I. Cirac, C. W. Gardiner, and P. Zoller, *Cold bosonic atoms in optical lattices*, Physical Review Letters **81** (1998), no. 15, 3108–3111.

[Joh84] Sajeev John, *Electromagnetic absorption in a disordered medium near a photon mobility edge*, Physical Review Letters **53** (1984), no. 22, 2169–2172.

[KA99a] G. Kopidakis and S. Aubry, *Intraband discrete breathers in disordered nonlinear systems. i. delocalization*, Physica D **130** (1999), 155–186.

[KA99b] G. Kopidakis and S. Aubry, *Intraband discrete breathers in disordered nonlinear systems. ii. localization*, Physica D **139** (1999), 247–275.

[KA00] G. Kopidakis and S. Aubry, *Discrete breathers and delocalization in nonlinear disordered systems*, Physical Review Letters **84** (2000), no. 15, 3236–3239.

[KKFA08] G. Kopidakis, S. Komineas, S. Flach, and S. Aubry, *Absence of wave packet diffusion in disordered nonlinear systems*, Physical Review Letters **100** (2008), no. 8, 084103.

[KM93] B Kramer and A MacKinnon, *Localization: theory and experiment*, Reports on Progress in Physics **56** (1993), no. 12, 1469–1564.

[Lan70] Rolf Landauer, *Electrical resistance of disordered one-dimensional lattices*, Philosophical Magazine **21** (1970), no. 172, 863–867.

[LFM+05] J. E. Lye, L. Fallani, M. Modugno, D. S. Wiersma, C. Fort, and M. Inguscio, *Bose-Einstein condensate in a random potential*, Physical Review Letters **95** (2005), no. 7, 070401.

[Llo69] P. Lloyd, *Exactly solvable model of electronic states in a three-dimensional disordered Hamiltonian: non-existence of localized states*, Journal of Physics C: Solid State Physics **2** (1969), no. 10, 1717–1725.

[LR85] Patrick A. Lee and T. V. Ramakrishnan, *Disordered electronic systems*, Review of Modern Physics **57** (1985), no. 2, 287–337.

[LR05] Benedict Leimkuhler and Sebastian Reich, *Simulating hamiltonian dynamics*, Cambridge University Press, 2005.

[MA94] R. S. MacKay and S. Aubry, *Proof of existence of breathers for time-reversible or hamiltonian networks of weakly coupled oscillators*, Nonlinearity **7** (1994), 1623–1643.

[MC08] R. V. Mishmash and L. D. Carr, *Ultracold atoms in 1d optical lattices: Mean field, quantum field, computation, and soliton formation*, arXiv **0810.2593v1** **[cond-mat.other]** (2008).

[Mot67] N. F. Mott, *Electrons in disordered structures*, Advances in Physics **16** (1967), no. 61, 49–144.

[Ott93] Edward Ott, *Chaos in dynamical systems*, Cambridge University Press, 1993.

[PF92] Leonid Pastur and Alexander Figotin, *Spectrum of random and almost periodic operators*, Springer-Verlag, 1992.

[PGK01] A. R. Bishop P. G. Kevrekidis, K. Rasmussen, *The discrete nonlinear schrödinger equation: A survey of recent results*, International Journal of Modern Physics B **15** (2001), no. 21, 2833–2900.

[PRTB82] M. A. Paalanen, T. F. Rosenbaum, G. A. Thomas, and R. N. Bhatt, *Stress tuning of the metal-insulator transition at millikelvin temperatures*, Physical Review Letters **48** (1982), no. 18, 1284–1287.

[PS08] A. S. Pikovsky and D. L. Shepelyansky, *Destruction of Anderson localization by a weak nonlinearity*, Physical Review Letters **100** (2008), no. 9, 094101.

[PTVF02] William H. Press, Saul A. Teukolsky, William T. Vetterling, and Brian P. Flannery, *Numerical recipes in C++*, Cambridge University Press, 2002.

[PV92] János Pipek and Imre Varga, *Universal classification scheme for the spatial-localization properties of one-particle states in finite, d-dimensional systems*, Physical Review A **46** (1992), no. 6, 3148–3163.

[Rén61] Alfréd Rényi, *On measures of entropy and information*, Proc. Fourth Berkeley Symp. on Math. Statist. and Prob., Univ. of Calif. Press, 1961, pp. 547–561.

[SBFS07] T. Schwartz, G. Bartal, S. Fishman, and M. Segev, *Transport and Anderson localization in disordered two-dimensional photonic lattices*, Nature (2007), 52–55.

[SDK+05] T. Schulte, S. Drenkelforth, J. Kruse, W. Ertmer, J. Arlt, K. Sacha, J. Zakrzewski, and M. Lewenstein, *Routes towards Anderson-like localization of Bose-Einstein condensates in disordered optical lattices*, Physical Review Letters **95** (2005), no. 17, 170411.

[She93] D. L. Shepelyansky, *Delocalization of quantum chaos by weak nonlinearity*, Physical Review Letters **70** (1993), no. 12, 1787–1790.

[She06] P. Sheng, *Introduction to wave scattering, localization and mesoscopic phenomena*, Springer-Verlag, 2006.

[Tho74] D. J. Thouless, *Electrons in disordered systems and the theory of localization*, Physics Reports **13** (1974), no. 3, 93–142.

[TP08] S. Tietsche and A. Pikovsky, *Chaotic destruction of Anderson localization in a nonlinear lattice*, EPL (Europhysics Letters) **84** (2008), no. 1, 10006 (5pp).

[Tuc76] B. Tuck, *Some explicit solutions to the non-linear diffusion equation*, Journal of Physics D: Applied Physics **9** (1976), no. 11, 1559–1569.

[vMBFR83] S. von Molnar, A. Briggs, J. Flouquet, and G. Remenyi, *Electron localization in a magnetic semiconductor*, Physical Review Letters **51** (1983), no. 8, 706–709.

[WBLR97] Diederik S. Wiersma, Paolo Bartolini, Ad Lagendijk, and Roberto Righini, *Localization of light in a disordered medium*, Nature (1997), 671–673.

[Ż03] K. Życzkowski, *Rény extrapolation of Shannon entropy*, Open Sys. & Information Dyn. **10** (2003), 297–310.

Acknowledgement

At first, I would like to thank Prof. Pikovsky who gave me the possibility of writing this Diploma thesis and assisted me through his advice as well as his actions. I also thank Prof. Shepelyansky from Toulouse for inviting me to France where some of the results presented in this thesis were found. Furthermore, I thank my colleague Karsten Ahnert for the many fruitful discussions and the helpful comments during the whole period of my work on this thesis. The same thanks go to Dr. habil. Abel and many other colleagues who supported my work with comments and advice. I also have to thank my friend David Zwicker and my father Bernd Mulansky for the proof-reading of this thesis and for providing me hints and corrections.

Last but not least, I thank my girlfriend Silke for her patience and encouragement during this time. Without her, I would not have written this thesis in Potsdam.

Erklärung

Hiermit erkläre ich, dass ich diese Arbeit im Rahmen der Betreuung im Institut für Physik und Astronomie der Universität Potsdam ohne unzulässige Hilfe Dritter verfasst und alle Quellen als solche gekennzeichnet habe.

Mario Mulansky

Potsdam, den 10. Juni 2009